

A census of young stellar population associated with the Herbig Be star HD 200775

Piyali Saha^{1,2*}, Maheswar, G¹, Kamath, U. S.¹, Lee, C. W³, Manoj, P.⁴,
Blesson Mathew⁵, Ekta Sharma¹

¹Indian Institute of Astrophysics (IIA), Sarjapur Road, Koramangala, Bangalore 560034, India

²Pt. Ravishankar Shukla University, Amanaka G.E. Road, Raipur, Chhatisgarh 492010, India

³Korea Astronomy, and Space Science Institute (KASI), 776 Daedeokdae-ro, Yuseong-gu, Daejeon 305-348, Republic of Korea

⁴Tata Institute of Fundamental Research, Homi Bhabha Road, Mumbai 400 005, India

⁵Department of Physics and Electronics, CHRIST (Deemed to be University), Bangalore 560029, India

Accepted XXX. Received YYY; in original form ZZZ

ABSTRACT

The region surrounding the well-known reflection nebula, NGC 7023, illuminated by a Herbig Be star, HD 200775, located in the dark cloud L1174 is studied in this work. Based on the distances and proper motion values from *Gaia* DR2 of 20 previously known young stellar object candidates, we obtained a distance of 335 ± 11 pc to the cloud complex L1172/1174. Using polarization measurements of the stars projected on the cloud complex, we show additional evidence for the cloud to be at ~ 335 pc distance. Using this distance and proper motion values of the YSO candidates, we searched for additional comoving sources in the vicinity of HD 200775 and found 20 new sources which show low infrared excess emission and are of age ~ 1 Myr. Among these, 10 YSO candidates and 4 newly identified comoving sources are found to show X-ray emission. Three of the four new sources for which we have obtained optical spectra show H α in emission. About 80% of the total sources are found within ~ 1 pc distance from HD 200775. Spatial correlation of some of the YSO candidates with the *Herschel* dust column density peaks suggests that star formation is still active in the region and may have been triggered by HD 200775.

Key words: Polarization – stars: distances, pre-main sequence – ISM: clouds – X-rays: stars

1 INTRODUCTION

A complete census of young stars and sub-stellar objects in the nearby star forming regions is essential to improve our understanding of the global properties of younger population like disc fraction, initial mass function, star formation efficiency and the star formation history. One of the key requirements to carry out such scientific investigations is the distance of the region from the Sun. It is an essential parameter required to determine many of the physically relevant properties such as the mass and the physical size of the molecular cloud. It is also required to determine the luminosity of young stellar objects (YSOs) that are embedded in the molecular cloud and the size of outflows, if present (Yun & Clemens 1990; Clemens et al. 1991; Kauffmann et al. 2008). Unfortunately, the distance estimation of many of the clouds is often plagued by very large uncertainties and it is seen in

the literature that measurements often differ by large factors, especially for those clouds that are isolated, sometimes by as much as a factor of two (Hilton & Lahulla 1995).

LDN 1172/1174 (hereafter L1172/1174; Lynds 1962) is an isolated star forming region situated at a relatively high Galactic latitude ($l \sim 104.1^\circ$, $b \sim 14.2^\circ$). L1172/1174 is associated with a bright reflection nebula NGC 7023 in the Cepheus constellation. The nebula is illuminated by a Herbig Be (B2/3Ve) star HD 200775 (The et al. 1994; Manoj et al. 2006) which is identified as a double-line spectroscopic binary system having primary and secondary masses of $10.7 \pm 2.5 M_\odot$ and $9.3 \pm 2.1 M_\odot$ respectively (Alecian et al. 2008). Being associated with a single filament, the whole cloud system resembles a “head-tail” structure oriented at an angle of $\sim 50^\circ$ to the Galactic plane (Elmegreen & Elmegreen 1978). An outflow from HD 200775, currently inactive though, is responsible for generating an asymmetric east-west biconical cavity that is filled with hot atomic gas (Fuente et al. 1998b). Rector & Schweiker (2013) discovered

* E-mail: s.piyali16@gmail.com (PS)

four new Herbig-Haro (HH) objects in NGC 7023 by wide-field imaging. At least two distinct outflows were discovered in the northwestern “lobe” of NGC 7023. [Kirk et al. \(2009\)](#) identified a total of 50 YSO candidates in the vicinity of HD 200775 based on the *Spitzer* Infrared Array Camera (IRAC) and the Multiband Imaging Photometer for *Spitzer* (MIPS) study of the Cepheus Flare. HD 200775 is located at the center of a sparse cluster of T Tauri stars (TTS; [Weston 1953](#)). Observationally, TTS are identified based on their proximity to molecular clouds and presence of Balmer lines of hydrogen in emission ([Appenzeller & Mundt 1989](#)). The equivalent width of H α emission line, EW(H α), is used to classify the TTS to classical (CTTS) and weak-line (WTTS) sources. About 14 of the TTS found near HD 200775 show H α in emission and variability. At least 3 of these TTS are found to be in binary systems ([Romano 1975](#)). Based on ^{13}CO observations, [Yuan et al. \(2013\)](#) suggested that strong winds from HD 200775 are blowing away ambient material causing further compression of the matter around it, especially to the northern region where most of the YSOs are found to be distributed. They also found a systematic decrease in the age of YSOs as a function of distance from HD 200775 implying that at least some of them are possibly formed as a result of the feedback from HD 200775. Presence of a Herbig Be star, HH objects and low mass YSOs makes L1172/1174 an excellent candidate to study star formation possibly due to stellar feedback.

The distance to L1172/1174 is not firmly constrained. Several values of distances have been quoted in the literature. The distance estimates made for the complex are compiled from literature and listed in Table 1. The estimated distances range from ~ 300 pc to ~ 700 pc. Based on the extinction and the absolute magnitude of HD 200775, [Viotti \(1969\)](#) made initial estimates of the distance to the star and obtained a value of 400 ± 100 pc. Using photoelectric photometry and low resolution spectroscopy of 75 stars projected against L1172/1174, [Shevchenko et al. \(1989\)](#) reported a distance of 300 ± 20 pc by producing a colour-excess vs distance plot. [Straizys et al. \(1992\)](#) used Vilnius photometry which gives two-dimensional classification and interstellar reddening produced extinction vs. distance plot of 79 stars towards the cloud. They obtained a distance of 288 ± 25 pc to L1172/1174. The parallax measurements of HD 200775 were used to calculate a distance of 430_{-90}^{160} pc to it ([van den Ancker et al. 1998](#)). However, based on a recomputed Hipparcos parallax value, [van Leeuwen \(2007\)](#) estimated a distance of 520_{-110}^{180} pc to HD 200775. [Maheswar et al. \(2010\)](#), by using 2MASS *JHK* photometry obtained extinction and distances of sources projected against the cloud, estimated a distance of 408 ± 76 pc. [Benisty et al. \(2013\)](#) obtained a revised distance of 320 ± 51 pc to HD 200775 by combining radial velocity measurements and astrometric data. Using Wolf diagrams, [Kun \(1998\)](#) suggested that the Cepheus region above the Galactic latitude of 10° consists of different cloud material partly projected against each other. They found evidence of absorbing clouds at ~ 200 and ~ 400 pc and assigned a distance of 450 ± 45 pc to L1172/1174. Evidence for the presence of two layers of interstellar gas was found in neutral hydrogen ([Heiles 1967](#)) and in CO molecular line ([Grenier et al. 1989](#)) observations. By applying kinematical method to velocity profiles of the lines, [Grenier et al. \(1989\)](#) estimated an approximate distances of 300 pc and 800

Table 1. List of previous distance estimation of L1172/1174 compiled from the literature.

Distance (pc)	Methods used to obtain the distance	Ref.
$282\pm 42^\dagger$	Extinction vs distance	1
288 ± 25	Extinction vs distance	2
300 ± 20	Color-excess vs distance	3
320 ± 51	Radial velocity and astrometry of HD 200775	4
358 ± 31	Distances of YSOs in Cepheus flare region	5
408 ± 76	Extinction vs distance (<i>JHK</i> photometry)	6
430_{-90}^{160}	<i>Hipparcos</i> distance of HD 200775	7
440 ± 100	Extinction and absolute magnitude of HD 200775	8
450 ± 45	Wolf diagrams	9
510 ± 130	Star counts method	10
520_{-110}^{180}	Recomputed <i>Hipparcos</i> distance of HD 200775	11
$715\pm 110^\dagger$	Extinction vs distance	1

1. [Zdanavičius et al. \(2009\)](#), 2. [Straizys et al. \(1992\)](#), 3. [Shevchenko et al. \(1989\)](#), 4. [Benisty et al. \(2013\)](#), 5. [Dzib et al. \(2018\)](#), 6. [Maheswar et al. \(2010\)](#), 7. [van den Ancker et al. \(1998\)](#), 8. [Viotti \(1969\)](#), 9. [Kun \(1998\)](#), 10. [Armandroff & Herbst \(1981\)](#), 11. [van Leeuwen \(2007\)](#)

† [Zdanavičius et al. \(2009\)](#) identified two layers of material towards the direction of L1172/1174 based on the jump in extinction seen in the extinction vs distance plot.

- 900 pc to the layers. [Zdanavičius et al. \(2009\)](#) investigated $1.5^\circ \times 1.5^\circ$ area centering at $l=104.1^\circ, b=14.2^\circ$. This area was divided into five smaller subareas and dependence of extinctions on distances were studied by using stars projected on these subareas. They suggested that the dust clouds in the vicinity of NGC 7023 are concentrated in at least two layers that are at ~ 280 pc and ~ 715 pc. However, in their analysis, the number of stars used to discern the hikes in extinction in different subareas is very small making the distance estimates quite uncertain.

On the basis of the spectral slope of their spectral energy distribution (SED) in the near- to submillimeter wavelengths, the YSOs are also classified on an empirical sequence into Class 0 - III and flat spectrum sources ([Lada 1987](#); [Andre et al. 1993](#); [Greene et al. 1994](#); [Robitaille et al. 2007](#); [Evans et al. 2009](#); [McClure et al. 2010](#)). The Class II and Class III objects generally correspond to CTTS and WTTS, respectively. Based on the H α emission, near-IR and mid-IR observations, a total of ~ 60 YSO candidates have been identified so far in NGC 7023 ([Kun et al. 2009](#); [Kirk et al. 2009](#); [Yuan et al. 2013](#)). Because WTTSs show low EW(H α) and less IR excess emission, it is difficult to distinguish them from the unrelated field stars and they may fail detection in H α and IR surveys. Thus a complete census of Class III sources in a star forming region may not always be complete. Using proper motion and parallax measurements from *Gaia* DR2, numerous kinematically coherent associations of stars have been recognized within a few hundred parsec of the Sun (e.g., [Dzib et al. 2018](#); [Luhman et al. 2018](#); [Faherty et al. 2018](#)). Detailed study of the nearest of these associations has revealed the presence of a large number of low mass stars and sub-stellar objects ([Luhman 2018](#); [Luhman et al. 2018](#)). Thus, an alternative way to get census

of disc-less young members, if present, in a star forming region is to look for additional sources that are kinematically associated with the known YSOs of the region. We made a search for any additional sources that may be comoving with the known YSO candidates and may have been missed detection in the earlier studies of L1172/1174 (Kun et al. 2009; Kirk et al. 2009; Yuan et al. 2013), using distance and proper motion values from the *Gaia* DR2 database.

In this work we estimated the distance to LDN 1172/1174 using recently released *Gaia* DR2 data of the YSO candidates identified in the direction of the cloud and of the sources for which we have made R-band polarimetric observations. Using the distances and the proper motion values of the YSO candidates as reference, we searched for additional co-moving sources in the cloud. We obtained a number of sources moving in a similar fashion as the YSO candidates and lying in a similar distance. We classified these comoving sources based on the additional information collated from the archives. The paper is organized in the following manner: details of our observations and the *Spitzer* and the *Gaia* DR2 data sets are described in section 2; results and discussion are presented in section 3. Finally, we conclude the paper with a summary of the results in section 4.

2 OBSERVATION AND DATA REDUCTION

2.1 Polarization measurements

The polarimetric observations of 42 fields covering the cloud L1172/1174 were carried out using ARIES Imaging Polarimeter (AIMPOL; Rautela et al. (2004)) mounted at the Cassegrain focus of 1.04m Sampurnanand Telescope, ARIES, Nainital, India. Observations were performed on 26 nights spanning over three years from 2015 to 2017 (see Table 2). The frames were obtained using a 1024×1024 pixel² CCD chip (Tektronix TK1024), of which central 325×325 pixel² area was used for imaging polarimetry. The plate scale of the CCD is 1.48 arcsec pixel⁻¹ and the FOV is $\sim 8'$. The full width at half maximum (FWHM) of the observed stellar image profile is found to be ~ 3 pixels. The read-out noise and the gain of the CCD were 7.0 e⁻¹ and 11.98 e⁻¹ per Analog to Digital Unit, respectively. A R-band filter, matching the Kron-Cousin passband ($\lambda_{eff} = 0.760$ μ m), was used during the observations. AIMPOL provides only linear polarization and consists of an achromatic half wave plate (HWP) acting like a modulator and a Wollaston prism as a beam splitter. This set up provides two images (ordinary and extraordinary) of each target on the CCD frame. The HWP is rotated to obtain four normalized Stokes parameters, $q[R(0^\circ)]$, $u[R(22.5^\circ)]$, $q1[R(45^\circ)]$ and $u1[R(67.5^\circ)]$, corresponding to its four positions, i.e. 0° , 22.5° , 45° and 67.5° . We estimate the errors in normalized Stokes parameters $\sigma_R(\alpha)(\sigma_q, \sigma_u, \sigma_{q1}, \sigma_{u1})$ in per cent using the relation given by Ramaprakash et al. (1998). The average background counts have also been estimated around ordinary and extraordinary images of each star (Ramaprakash et al. 1998).

The contribution of instrumental polarization from the measurements was removed by observing a number of unpolarized standard stars from Schmidt et al. (1992). We

Table 2. Log of observations.

Year	Month (Date)
Polarimetric Observations	
2015	Oct (11), Nov (2, 3, 15, 16, 17), Dec (15)
2016	Oct (23, 25, 26, 27, 28), Nov (22, 26, 27)
2017	May (22, 23), Oct (13, 14, 17, 18, 19, 20, 21, 26, 27)
Spectroscopic Observations	
2018	Oct (11), Nov (30)

also observed six polarized standard stars (HD 236633, BD+59°389, HD 19820, HD 204827, HD 25443, HD 15445) from the list given by Schmidt et al. (1992) to determine the reference direction of the polarizer during our observing runs. The measurements were used to obtain the zero-point offset with respect to the north, which was later applied to the position angles of the observed stars. After bias subtraction, flat correction of the images using the flux normalization formula from Ramaprakash et al. (1998), we aligned and combined multiple images of a given field. The selection of the ordinary and extraordinary pair of each star from a given field was automated using a program written in the Python language. We performed photometry of the selected pairs using the Image Reduction and Analysis Facility (IRAF) DAOPHOT package to obtain the P% and position angle (θ_P) of each star. The details of the instrument used and data reduction procedure are given in Soam et al. (2013, 2015, 2017).

2.2 Spectroscopic Observations

We carried out spectroscopic observations of 4 of the 20 newly identified co-moving sources discussed in this work using the Hanle Faint Object Spectrograph Camera (HFOSC) mounted on the 2-m Himalayan Chandra Telescope (HCT) of the Indian Astronomical Observatory (IAO). We selected sources based on their relative brightness. The HFOSC is equipped with a $2k \times 4k$ SITE CCD chip. We used a combination of slit 1671 (slit width 1.92 arcsec $\times 11$ arcmin) and grism 7, covering the wavelength range 3500 - 7500 \AA . This slit and grism combination gives a spectral resolution of $\Delta\lambda \sim 8$ \AA . All the pre-processing and data reduction were performed in the standard manner using various tasks available with the IRAF. We used “splot” task to obtain the equivalent width of our observed sources. The log of the observations is given in Table 2.

2.3 *Spitzer* photometry of point sources

The *Spitzer* photometry of the known YSO candidates are obtained from the literature (Kirk et al. 2009). For the newly identified comoving sources, we calculated the *Spitzer* IRAC (3.6, 4.5, 5.8, 8.0 μ m) magnitudes by carrying out photometry on the images obtained from the *Spitzer* Space Observatory archive with Program ID: 30574 (Kirk et al. 2009). The basic calibrated data (BCD) frames were co-added and mosaic images were created using the SSC mosaicing and point-source extraction software (MOPEX; Makovoz & Marleau 2005). Sources were extracted from the final images using

MOPEX. Photometry was performed by extracting the flux using an aperture of 7 pixels wide box centered on each source using the APEX tool developed by the *Spitzer* Science Center. For the sources for which APEX failed to detect in automated mode at one or more wavelengths, we used the user list option to supply the coordinates of the source to obtain the flux values. We adopted 280.9, 179.7, 115.0 and 64.1 Jy in the 3.6, 4.5, 5.8 and 8.0 μm bands, respectively as the zero points for conversion between flux densities to the magnitudes as provided by Kirk et al. (2009).

2.4 The *Gaia* DR2 data

Gaia DR2 provides accurate positions, parallaxes and proper motions for more than a billion objects (Gaia Collaboration et al. 2018a,b). However, the conversion from parallax to distance is known to become non-trivial when the observed parallax is small compared to its uncertainty especially in cases where $\sigma_{\varpi}/\varpi \gtrsim 20\%$ (Bailer-Jones 2015). Recently, Bailer-Jones et al. (2018) calculated distances to 1.331 billion sources for which *Gaia* measured parallaxes by adopting an exponentially decreasing space density prior in distance. The distances to the YSO candidates and the field stars for which we made polarization measurements are obtained from Bailer-Jones et al. (2018) and proper motions from Gaia Collaboration et al. (2018a).

3 RESULTS AND DISCUSSION

3.1 Distance to L1172/1174

3.1.1 Distance based on the known YSO candidates associated with the cloud

One of the direct ways of estimating distances to a molecular cloud is to use the stars that are associated with the cloud. Recently, using 47 YSO candidates identified by Kun et al. (2008), Dzib et al. (2018) estimated a distance of 358 ± 32 pc to the whole Cepheus flare region. But as discussed by Kun (1998), the Cepheus flare region contains clouds that are located at different distances in projection. The distances of YSOs studied by Dzib et al. (2018) also show a large spread ranging from ~ 200 pc to ~ 400 pc. Therefore, in this work, we restricted our analysis to sources that are located within a $1^\circ \times 1^\circ$ region about the star HD 200775 and estimated the distance to L1174.

A total of 58 YSO candidates have been identified till now (after taking into account the common sources among various studies) in the vicinity of L1172/1174 (Kirk et al. 2009; Kun et al. 2009; Yuan et al. 2013). Of the 58 YSO candidates, we found distance and proper motion values in the right ascension ($\mu_{\alpha\star} = \mu_{\alpha} \cos \delta$) and declination (μ_{δ}) for 37 sources in the Bailer-Jones et al. (2018) and in the *Gaia* DR2 (Gaia Collaboration et al. 2018a) catalogues, respectively. For all the 37 sources, a *Gaia* counterpart was found well within $1''$ of the input coordinate of the YSO candidates and the ratio, m/σ_m (here m represents the distance, $\mu_{\alpha\star}$ and μ_{δ} values and the σ_m represents their respective errors) ≥ 1 . The *Gaia* DR2 results for the YSO candidates are shown in Fig. 1. The triangles and circles represent the distance- $\mu_{\alpha\star}$ and distance- μ_{δ} values respectively. Of the 37, 6 sources (red circles and triangles) are with $1 \leq m/\sigma_m < 2$; 8 sources (blue

circles and triangles) are with $2 \leq m/\sigma_m < 3$; and 23 sources (green circles and triangles) with $m/\sigma_m \geq 3$. The distance- $\mu_{\alpha\star}$ and distance- μ_{δ} values for the HD 200775 are identified and marked separately. Three sources out of these 23 are found to be at a distance greater than 1 kpc. Thus, in this work, we selected only those sources for which $m/\sigma_m \geq 3$ and are at distances less than 1 kpc. The results of these sources (20) are shown in Table 3.

Based on the proper motion and the distance values, a clear clustering of sources are evident in Fig. 1. The median of $\mu_{\alpha\star}$, μ_{δ} and distance values are 7.301 mas/yr, -1.619 mas/yr and 335 pc, respectively. The variance and the standard deviation that are commonly used to measure spread in a data are more affected by the extreme (high and low) values. Therefore here we used median absolute deviation (MAD) to estimate statistical dispersion which is more resilient to outliers in a data set than the standard deviation. The estimated MAD in distance, $\mu_{\alpha\star}$ and μ_{δ} are 11 pc, 0.386 mas/yr and 0.427 mas/yr, respectively. A majority of the YSO candidates (14) are found to fall within the constraints of three times the MAD in proper motions and distances as shown in Fig 1 using the ellipses drawn with darker shade. Two more sources get included when we consider a constraint of five times the MAD in proper motions and distances (ellipses drawn in lighter shade). Remaining four sources show large scatter from the median values. We note that HD 200775 is showing a larger distance ($\sim 2 \times$ MAD) with respect to the median value. In column 9 of Table 3, we give the renormalized unit weight error (RUWE¹; Lindegren 2018) for the YSO candidates. RUWE is a scaled unit weight error (UWE) with the scaling factor depending on the magnitude and color of the sources. Theoretically, the UWE is expected to be close to 1.0 for well-fitted solutions of single stars but can show larger values depending on the source environment and the geometric properties such as binarity. Practically, sources showing RUWE ≤ 1.4 are considered as having good astrometric solution (Lindegren 2018). As can be noticed, of the 20 YSO candidates, 10 sources show RUWE > 1.4 . The four sources showing large scatter from the median values are the ones showing relatively high values of RUWE (> 3.0). Of the remaining six, except one, the others show RUWE in the range of 1.5-1.6, including HD 200775 which shows a marginally higher value of 1.6. Thus we considered all the 16 sources that are lying within $5 \times$ MAD limit as part of L1174 and sources (four of them) that are located outside of the $5 \times$ MAD ellipses are considered as outliers. The distance of 335 ± 11 pc (the MAD is taken as the uncertainty in the distance) to L1174 implies that L1174 is at a height of ~ 80 pc above the galactic mid-plane. This is higher when compared to the scale-heights of ~ 45 pc estimated for the OB stars in the local galactic disc (Reed 2000) and for the molecular gas (e.g. Heyer & Dame 2015). Thus, L1174 is an example of a sparse cluster of young stars (which contains one or two intermediate mass stars) forming at a relatively high galactic latitude.

¹ RUWE values are obtained from <http://gaia.ari.uni-heidelberg.de/>

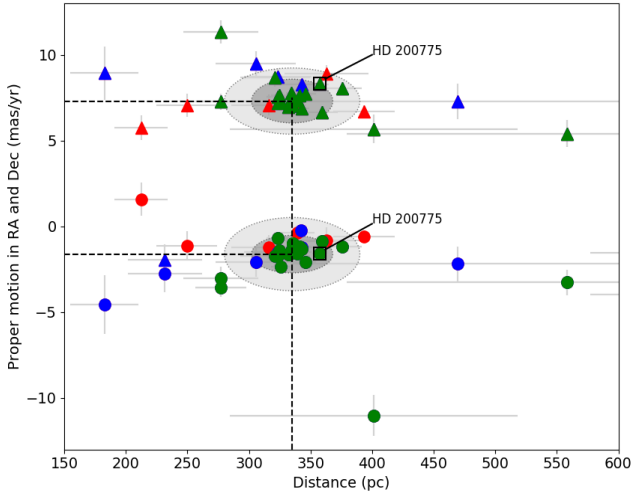


Figure 1. Proper motion values of the known YSO candidates associated with L1174 are plotted as a function of their distances obtained from *Gaia* DR2. The triangles and circles represent the distance- μ_{α^*} and distance- μ_{δ} values respectively. Location of HD 200775 is also marked. The error ellipses corresponding to $3 \times$ MAD (darker shade) and $5 \times$ MAD (lighter shade) in proper motion and distance values are drawn. The dashed lines show the median values of distance, μ_{α^*} and μ_{δ} . The ratios of distances and proper motion values with their respective errors $2 > (m/\sigma_m) \geq 1$ are for red points, $3 > (m/\sigma_m) \geq 2$ for blue points and $(m/\sigma_m) \geq 3$ for green points.

3.1.2 R-band polarization and the *Gaia* DR2 parallax measurements of field stars

Presence of interstellar dust grains along a given line of sight can be inferred by their effects on starlight coming from the background stars. Rotating non-spherical dust grains get aligned with their minor axis parallel to the ambient magnetic field (Davis & Greenstein 1951; Crutcher 2012). When the unpolarized starlight coming from a background star passes through regions containing such dust grains, the light gets polarized due to the selective absorption. Normally the value of P% increases gradually with the increase in the column of dust grains along the pencil-beam of a starlight. However, when it encounters a molecular cloud, a sudden increase in the values of P% occurs. Therefore, while the stars that are foreground to the cloud are expected to show low values of P%, the stars that are located behind the cloud are expected to show higher values of P%. The distance at which the sudden increase in the P% occurs is taken as the distance of the cloud (e.g. Straizys et al. 1992; Whittet et al. 1997; Knude & Hog 1998; Alves & Franco 2007). We examined the R-band polarization measurements of 569 sources that are projected on L1172/1174. The advantage of using polarization measurements to infer the presence of a molecular cloud is that the measured values are independent of the nature of the background stars.

The results of our polarization measurements for the stars are plotted in Fig. 2. The lengths of the vectors are proportional to the value of P% and the orientations depend on the θ_p . The values of θ_p are measured from the north increasing towards the east. We obtained *Gaia* DR2 distances for 545 sources from the Bailer-Jones et al. (2018) catalogue. In all the cases, we obtained a *Gaia* DR2 coun-

terpart within $1''$ of our source positions. The results are presented in Fig. 3. The P% vs. distance and θ_p vs. distance plots are shown in Fig. 3 (a) and (b), respectively using filled triangles in grey. We have shown only 301 sources for which the ratios of the P%, θ_p and distance and their corresponding error, P/σ_P , $\theta_p/\sigma_{\theta_p}$ and $d/\sigma_d \geq 3$, respectively. The mean values of P% and θ_p are found to be 2.5% and 142° . The closest star observed by us is at a distance of 306 pc. Therefore to investigate the foreground contribution to the polarization, we searched for additional sources in the Heiles (2000) catalogue with a search radius of 6° about HD 200775. The search gave a total of 26 sources of which HD 200775, HD 203467, HD 208947 and HD 193533 were not considered in the analysis due to the following reasons. The polarization values of HD 200775 could be affected by the reflection nebula around it. The HD 203467 is a Be type object, HD 208947 is an Algol variable and HD 193533 is classified as a variable source in the Simbad database. Of the 22, we obtained the *Gaia* DR2 distance for 17 sources from the Bailer-Jones et al. (2018) catalogue. The degree of polarization ($P_H\%$) and polarization position angles (θ_H) of the 17 sources are shown using filled circles in black in both (a) and (b) of Fig. 3 respectively. Because the foreground sources show relatively very low polarization, we set no constraints on the P_H/σ_H values while selecting them.

In Fig. 3 (a), the $P_H\%$ of the stars having distances less than ~ 335 pc (marked using dotted line in both upper and lower panels) show low values of polarization while the ones behind the cloud show relatively higher values. A significant increase in the P% values are seen at ~ 335 pc for the sources observed by us which confirms the presence of the cloud at that distance, similar to what we obtained from the YSO candidates. From the Fig. 3 (b), as the distance increases from ~ 100 pc to ~ 335 pc, the θ_H values are found to change systematically from $\sim 0^\circ$ to a value close to the mean value of 142° obtained for the sources observed by us. The mean value of the θ_H for the 4 sources lying beyond the distance of 335 pc is found to be $\sim 143^\circ$. Based on an abrupt increase in the values of the P% and the change in the θ_p for stars projected on the cloud, we confirm the distance of the entire L1172/1174 cloud complex at ~ 335 pc.

3.2 Additional comoving sources identified from the *Gaia* DR2 proper motion

With the knowledge of the precise values of position, proper motion and distance from the *Gaia* DR2 measurements, we looked for additional, probably young, sources that are comoving with the already known YSO candidates associated with L1172/1174. For this, we obtained proper motions and distances of sources that are located within a region of $1^\circ \times 1^\circ$ centered around HD 200775 from the *Gaia* DR2 and Bailer-Jones et al. (2018) catalogues, respectively. For the reason that the majority of the known YSO candidates are distributed within a region of $1^\circ \times 1^\circ$ centered around HD 200775, we conducted our search for the comoving objects also within the same area. As in the case of the YSO candidates, here again we selected only those sources for which $m/\sigma_m \geq 3$. Considering that a majority of the previously known YSO candidates are found within $5 \times$ MAD with respect to the median values of the distance and the proper

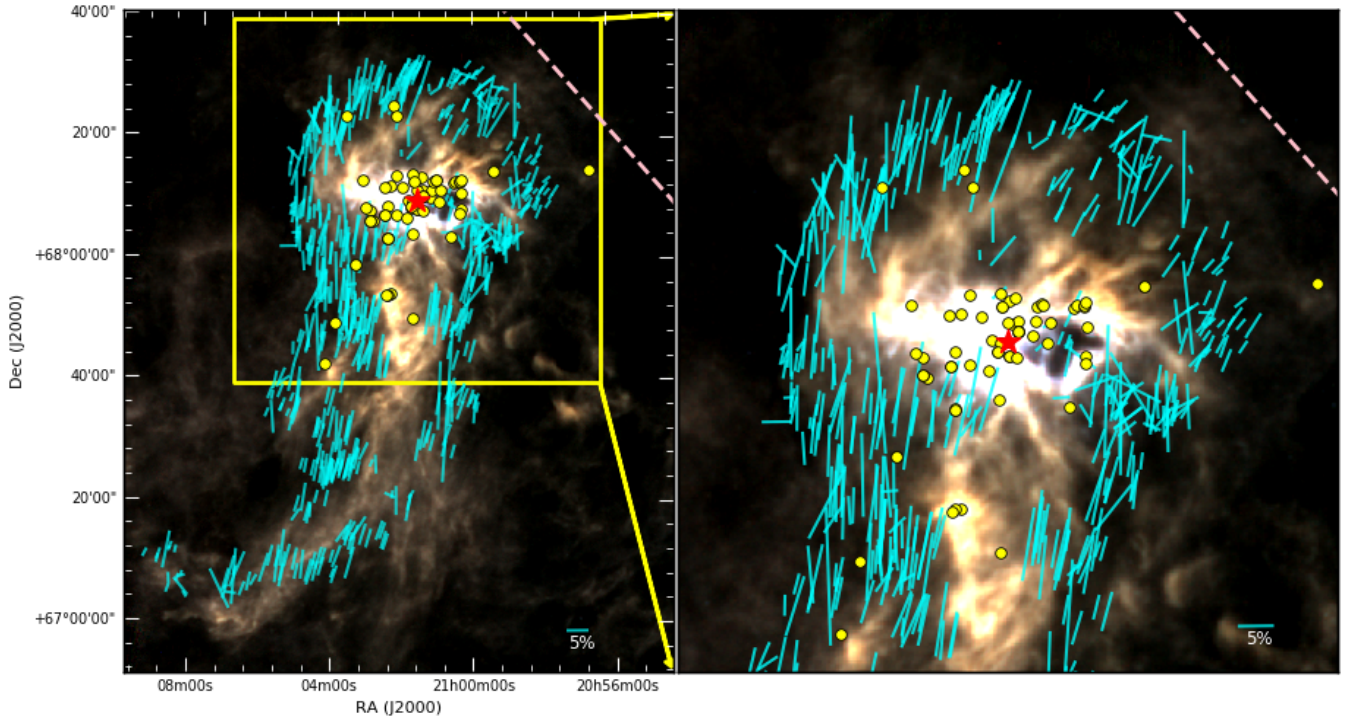


Figure 2. **LHS:** R-band polarization vectors (cyan lines), obtained from our observations, overplotted on *Herschel* colour-composite diagram with 250, 350 and 500 μm images. Broken line in pink represents the galactic plane. Locations of the known YSO candidates (yellow circles) around the central star HD 200775 (red star) are also shown. A polarization vector corresponding to 5% is shown for reference. **RHS:** Enlarged view of the $1^\circ \times 1^\circ$ region around HD 200775. Symbols represent the same as LHS.

motions, the same criteria are used to select the comoving sources also. That is, all sources falling within the range of $5 \times \text{MAD}$ with respect to the median values of the distance and the proper motions are regarded as comoving sources and included for further analysis.

The selected sources are shown on the proper motion – distance plot presented in Fig. 4 and results are tabulated in Table 4. The distance- $\mu_{\alpha\star}$ and distance- μ_{δ} values of the known YSO candidates are shown using filled triangles and filled circles in red, respectively. The same for the comoving sources are presented using filled triangles and filled circles in green, respectively. The ellipses drawn in grey in Fig. 4 represent the constraint of $5 \times \text{MAD}$ drawn at the median values of $\mu_{\alpha\star}$, μ_{δ} and distances of the known YSO candidates. Here again, the distance- $\mu_{\alpha\star}$ and distance- μ_{δ} values of HD 200775 are marked. We found a total of 20 additional sources that are located within the grey ellipses. The distance- $\mu_{\alpha\star}$ and distance- μ_{δ} values of these 20 additional sources are shown using filled triangles and filled circles in green respectively in Fig. 4. In Fig. 5 we show the $\mu_{\alpha\star}$ and μ_{δ} values of the known YSO candidates and the 20 additional sources using filled triangles in red and green respectively. HD 200775 is indicated by an orange star symbol. The grey ellipse indicates the range of $5 \times \text{MAD}$ in $\mu_{\alpha\star}$ and μ_{δ} about the median values obtained for the known YSO candidates. The kinematic association of the newly found 20 sources with the known YSO candidates is clearly evident in Fig. 4 and Fig. 5. The proper motion values of other sources (open circles) in the field are found to be very different. The positions of the known YSO candidates and the 20 additional sources that are comov-

ing are identified on the *Herschel* SPIRE 250 μm image as shown in Fig. 6 using red and green circles, respectively. The position of HD 200775 is shown using an orange star symbol. The arrows in red, green and orange show the proper motion directions of the known YSO candidates, newly identified comoving sources and HD 200775, respectively. Spatial locations of the comoving sources are very similar to those of the known YSO candidates. The distance and the proper motion values of the comoving sources are listed in Table 4. The RUWE value for the comoving sources are also shown in Table 4. Of the 20 comoving sources, only one source (c12) show RUWE of 1.5 which is marginally greater than the value of 1.4 considered as criterion for good solutions.

To investigate whether the sources with similar proper motions as that of the known YSO candidates from a given 1° square area are a chance projection of field stars or are really the comoving sources associated with the region, we selected 1° square area from three reference fields lying towards the direction of the southern (tail) part of L1172/1174 having similar declination but differing in right ascension (field 1: 318.79282° , 67.174828° ; field 2: 316.21048° , 67.206136° ; field 3: 313.56081° , 67.197843°). Here also, we selected only those sources that are with $m/\sigma_m \geq 3$. We found only one source (in field 1), HD 202461 (distance = 309_{-2}^3 pc, $\mu_{\alpha\star} = 7.317 \pm 0.060$ mas/yr and $\mu_{\delta} = -1.724 \pm 0.050$ mas/yr), which satisfies the above constraints (marked with a square box in the ellipses). Information pertaining to this source is not available in the literature. Thus, on an average, we expect at most one source in a given 1° square area in the direction close to L1172/1174 that could be a chance projection

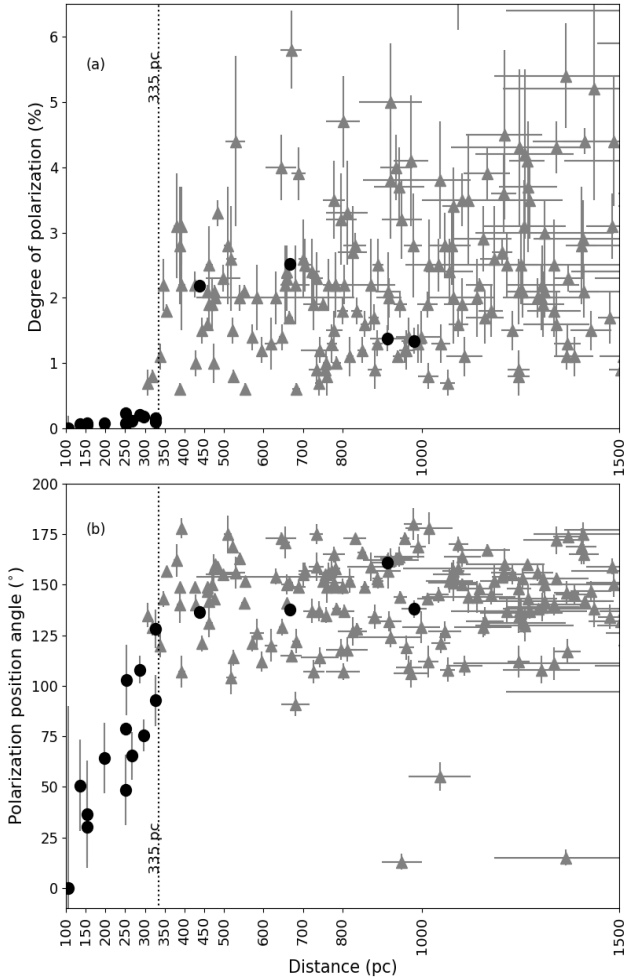


Figure 3. (a) Polarization (%) vs. distance plot for the stars projected towards the direction of L1172/1174 (filled triangles in grey). The filled circles in black are the sources for which the P% is obtained from the Heiles (2000) catalogue. (b) Polarization position angle vs. distance plot for the stars projected in the periphery of L1172/1174. The symbols are same as above.

of field stars having proper motions and distances similar to those of the known YSO candidates. This confirms the presence of an over-density of stars within 1 square degree around HD 200775.

3.3 Properties of the sources identified around HD 200775

3.3.1 X-ray properties

The field containing HD 200775 was observed by the *XMM-Newton* telescope to investigate X-ray properties of early type stars (Nazé et al. 2014). We searched for additional X-ray sources in the region around HD 200775 in the XMM-SSC, 2018 catalogue (Rosen et al. 2016). Within the FOV of the *XMM-Newton*, we found a total of 35 X-ray emitting sources. The maximum likelihood parameter is set at ≥ 15 (which gives the maximum likelihood of the source detection, López-Santiago & Caballero 2008), and the detection quality flag set at 0 or 1. The exposure time of the observations was 11.9 ks. Out of 35, 19 sources are found to have

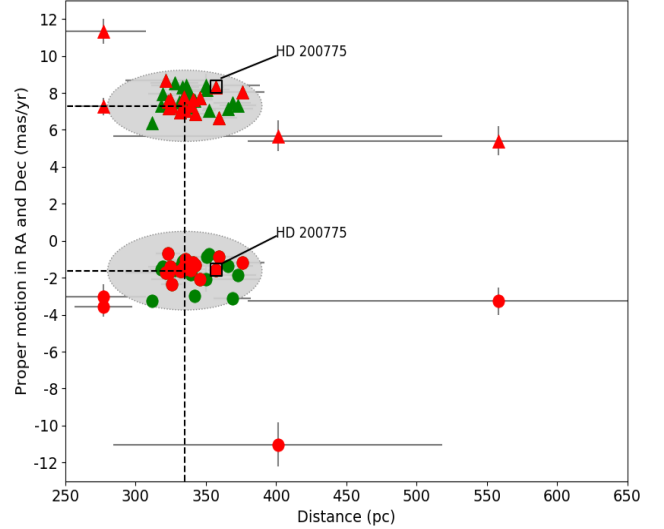


Figure 4. Proper motion vs. distance plot for the known YSO candidates (triangles and circles in red) and for the 20 newly identified comoving sources (triangles and circles in green). The triangles (red and green) and circles (red and green) represent the distance- μ_{α^*} and distance- μ_{δ} values of the known YSO candidates and comoving sources respectively. Locations of HD 200775 are identified by square boxes. The grey ellipses represent the boundary of the proper motion values and the distance ranges used to identify the new comoving sources. The dashed lines show the median values of distance, μ_{α^*} and μ_{δ} .

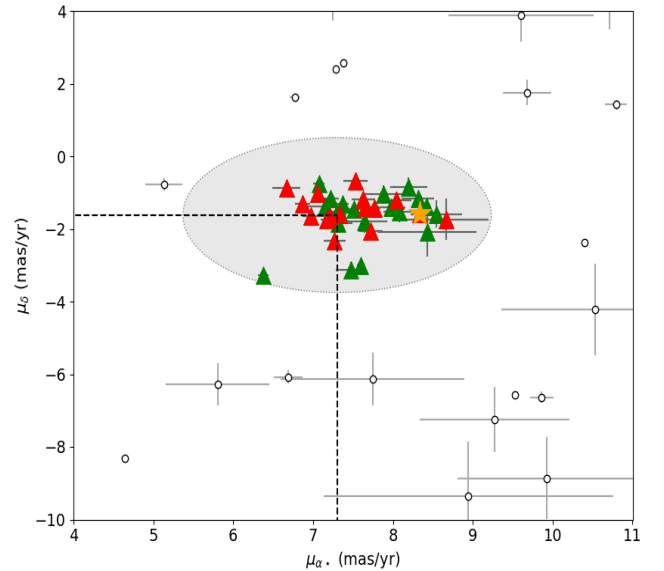


Figure 5. μ_{δ} vs. μ_{α^*} plot for the known YSO candidates and for the comoving sources. Red triangles represent proper motion values of known YSO candidates and green triangles represent that of the comoving sources. The grey ellipse represents the boundary of the proper motion values considered to select the comoving sources. The orange star symbol indicates the location of HD 200775. The open circles represent sources not satisfying the $5 \times \text{MAD}$ conditions in distance and proper motion values. The dashed lines show the median values of μ_{α^*} and μ_{δ} .

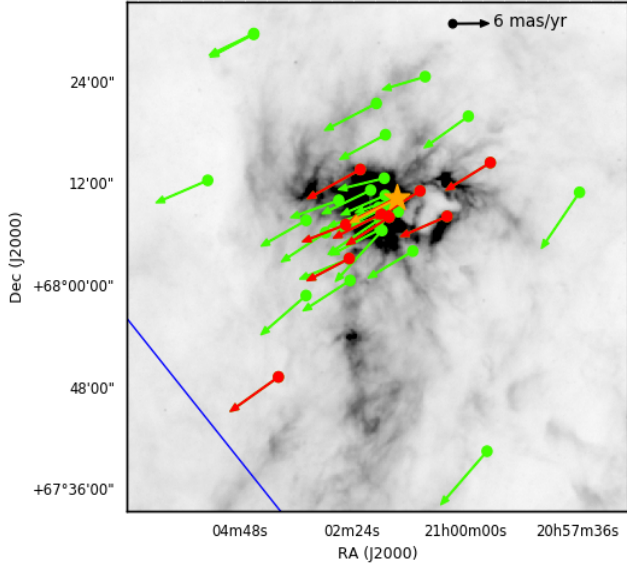


Figure 6. Proper motion plot for the YSO candidates (red arrows) associated with L1174 overplotted on the *Herschel* SPIRE 250 μm image. The green arrows represent the same for the newly identified comoving sources. HD 200775 is indicated by a star symbol and an arrow in orange. The blue solid line represents the galactic plane.

the ratio of the flux in 0.2–12 keV and the corresponding error ≥ 3 . Of these, 10 known YSO candidates (including HD 200775) and 4 newly identified comoving sources are found to spatially coincide within $5''$ from the positions of the X-ray detection. Based on the study conducted by Getman et al. (2011) on the Carina Nebula using the Chandra telescope and scaling for the survey coverage, approximately $\sim 10 - 20$ foreground and background and 30 extragalactic sources could be detected within the FOV of *XMM-Newton*. The foreground and background stars may have detection in *WISE*, but extragalactic sources may not have a *WISE* counterpart, because they are below its sensitivity limit. Out of 10 known YSO candidates, 8 of them have *WISE* counterparts. All the 4 newly identified comoving sources emitting in X-ray, have *WISE* counterparts.

The *XMM-SSC* catalogue provides hardness ratios, HR1 and HR2 also. These are X-ray colours defined as $(H-S)/(H+S)$ where H and S for HR1 are flux values in the band 0.5–1.0 keV and 0.2–0.5 keV respectively. For HR2, the H and S are flux values in the bands 1.0–2.0 keV and 0.5–1.0 keV respectively. Fig. 7 shows the HR2 vs HR1 plot for our YSO candidates (filled circles in green and black), 4 newly identified comoving sources (filled circles in cyan) and HD 200775 (star symbol in green). We obtained *XMM-Newton* data for the CTTS and WTTS taken from Wahhaj et al. (2010) which are shown using red and blue filled dots respectively. Herbig AeBe (HAeBe) sources taken from The et al. (1994) catalogue are shown using dots in green. As mentioned already, some of the X-ray detection found in the vicinity of HD 200775 could be background galaxies. To differentiate the background galaxies from the PMS stars based on their hardness ratios, we obtained *XMM-Newton* data around a $5''$ search radius of the galaxy samples of Barcons et al. (2007). This includes broad line active galactic nuclei, narrow emission line galaxies, absorption line galax-

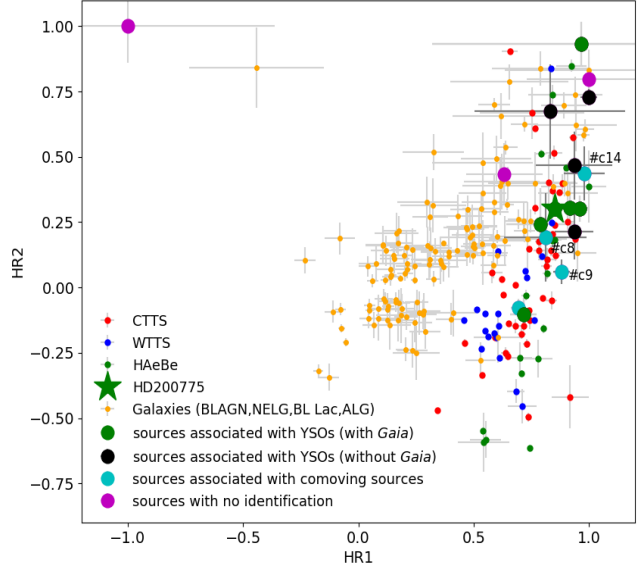


Figure 7. Hardness ratio plot for the X-ray sources detected by the *XMM-Newton* telescope in the vicinity of HD 200775. Known YSO candidates (with and without reliable *Gaia* data) and the newly identified comoving sources are identified. The comoving sources which are observed by us spectroscopically are marked. The hardness ratios of CTTS (red dots), WTTS (blue dots), HAeBe (green dots) and galaxies (orange dots) are also shown.

ies, BL Lacertae. These sources are shown using orange dots in Fig. 7.

The HAeBe, CTTS and WTTS (The et al. 1994; Wahhaj et al. 2010) are found to occupy a distinct region in Fig. 7. However, the distribution of the galaxy sample is noticeably different from that of the HAeBe, CTTS and WTTS. The HR1 colours of CTTS range between 0.5 - 1.0, while for WTTS, it is mostly close to ~ 0.6 . The HR2 colours for CTTS show large range (0.5 to -0.5), while WTTS predominantly show $\text{HR2} \lesssim 0.5$. The known YSO candidates and the comoving sources found associated with the X-ray detection are distributed in a similar manner as that of HAeBe, CTTS and WTTS. Here our aim is not to characterize their X-ray properties but to show that X-ray sources found in the vicinity of HD 200775 show X-ray colours similar to those of CTTS and WTTS. Of the 5 X-ray detections that are not associated with any of the known YSO candidates or the comoving sources, 2 of them, namely, #x1 and #x5 (the identification numbers are as given in Table 5) do not have 2MASS, *Spitzer* and *WISE* counterparts within $5''$ search radius. The location of #x1 at $(-1.0, 1.0)$ is conspicuously different from the rest of the sources in Fig. 7 while the source #x5, located at $(1.0, 0.8)$, could possibly be an extragalactic source due to the lack of *WISE* detection. Among the 3 sources with *WISE* counterparts, #x2 which is located at $(0.63, 0.43)$ in Fig. 7 shows hardness ratios consistent with those of the extragalactic sources. The sources #x3 and #x4, based on the *Gaia* DR2 distances, are foreground sources and hence not shown in the figure. Two *Gaia* counterparts are found within our search radius of $5''$ for #x3. The high proper motions ($\mu_{\alpha^*} = -2.492$ mas/yr and -4.615 mas/yr and $\mu_{\delta} = -34.948$ mas/yr and -34.931 mas/yr) confirm that they are foreground. #x4 with $\mu_{\alpha^*} = 8.628$ mas/yr and $\mu_{\delta} = 5.798$

mas/yr, confirms that this source is kinematically not associated with the region. Therefore we did not consider any of the X-ray sources other than those associated with the known YSO candidates and the comoving sources in further analysis.

3.3.2 Spectroscopy of four comoving sources

Of the 20 newly identified comoving sources, we obtained spectroscopic observations for four of them during our recent observing run. The objective was, as a first step, to look for emission lines in them. Spectral types of the four sources were determined by comparing the features in the spectrum of our sources with those in the templates of main sequence stars from the stellar library provided by [Jacoby et al. \(1984\)](#). Before performing the comparison, we normalized the spectra of our sources and took the templates to a common resolution. The uncertainty in our spectral classification is found to be of two spectral subclasses. The stars #c8 and #c18 (star identification numbers are as given in Table 4) are found to be of M1 spectral type while #c14 is found to be of M3 spectral type. The observed spectra of star #c8, #c14 and #c18 are shown in Fig. 8. All the three are found to be X-ray emitters. We detected H α in emission in all three of them. We used the SPLIT task in the IRAF to obtain EW(H α) of our observed sources. The EW(H α) of #c8 and #c18 are found to be -15.03 ± 1.52 Å and -13.01 ± 1.30 Å, respectively. According to [Barrado y Navascués & Martín \(2003\)](#), these two sources can be classified as CTTS. However, it is surprising that these sources were not detected in any of the earlier surveys for H α emission stars. Variability of H α emission in #c8 and #c18 could be a plausible reason. The EW(H α) of #c14 is found to be -4.06 ± 0.41 Å which could possibly be a WTTS as mentioned in [Barrado y Navascués & Martín \(2003\)](#). The fourth star, #c9, is having H α in filled-in emission. This star is found to be of a K2 spectral type. To reveal its H α emission, we have subtracted the spectrum of a main sequence K2 spectrum (red) from that of the source #c9 (black) as shown in Fig. 9. The resultant spectrum is shown in green. The EW(H α) obtained from the resultant spectrum is found to be -0.69 ± 0.08 Å.

3.3.3 NIR and Mid-IR properties

To understand the nature of the newly identified comoving sources based on their near and mid-infrared colours, we obtained their 2MASS and *Spitzer* magnitudes. The 2MASS magnitudes are obtained from [Cutri et al. \(2003\)](#). Sources having photometric quality ‘A’ (SNR ≥ 10) in *J*, *H* and *K_S* are selected. Out of 20 comoving sources, we found a 2MASS counterpart for 19 of them. Of the 20 known YSO candidates having reliable *Gaia* DR2 data (Table 3), we found a 2MASS counterpart for 17 of them. We used a search radius of 1'' for getting the 2MASS counterparts. The comoving sources and the known YSO candidates are shown in the (*J-H*) vs. (*H-K_S*) colour-colour (CC) diagrams in Fig. 10 using filled circles in cyan and green, respectively and listed in Table 6. Also shown are the positions of Class I, II and III (red, maroon and blue dots, respectively) sources taken from [Rebull et al. \(2010\)](#) for comparison. The four sources for which we made optical spectroscopic observations (discussed in section 3.3.2) are identified and labeled. Of the

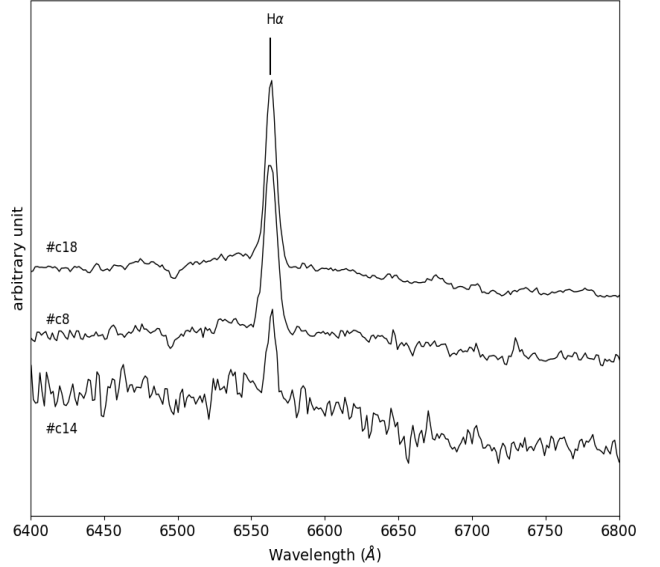


Figure 8. Spectra of 3 of the 4 newly identified comoving sources found around HD 200775. The source identification numbers are also given. Wavelengths corresponding to H α lines are marked with dashed vertical lines.

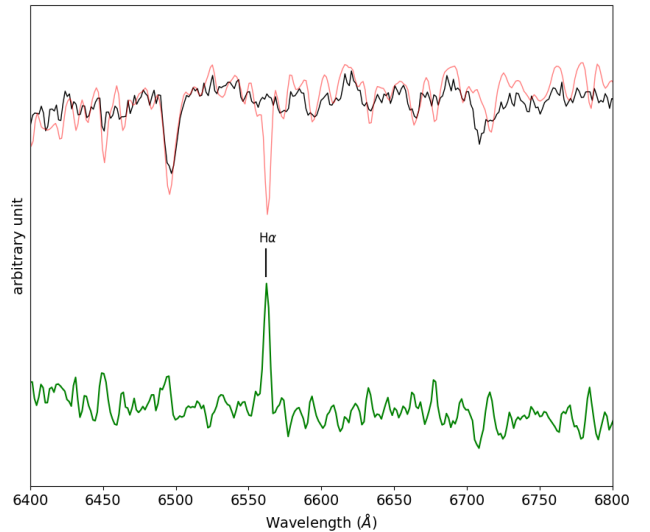


Figure 9. Spectrum of the comoving source #c9 (black) overplotted with a K2 spectral type spectrum (red) from [Jacoby et al. \(1984\)](#). The subtracted spectrum (#c9-K2) shown in green reveals the filled-in emission in the observed spectrum of #c9.

remaining 38 known YSO candidates lacking reliable data or detection by the *Gaia*, we obtained the 2MASS magnitudes for 28 sources. The results are presented in Table 7 and shown in Fig. 10 using filled circles in black. The known YSO candidates and the newly identified comoving sources that are spatially associated with the X-ray detection made by the *XMM-Newton* satellite are identified using open square symbols in magenta.

The distribution of the known YSO candidates in the (*J-H*) vs. (*H-K_S*) CC diagram as shown in Fig. 10 is found to be similar to that of the Class I and Class II (red and maroon dots, respectively) sources taken from [Rebull et al. \(2010\)](#).

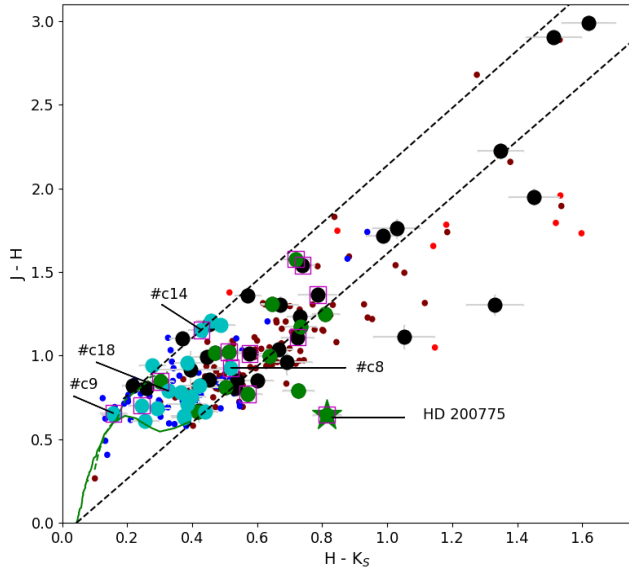


Figure 10. The $(J-H)$ vs. $(H-K_S)$ CC diagram for the newly identified comoving sources shown using filled cyan circles. The known YSO candidates having reliable *Gaia* data (green circle) and those without reliable *Gaia* data or no detection (black circle) are also shown. The solid curves in green represent the loci of the unreddened main sequence stars and the giants. The Class I, II and III sources taken from [Rebull et al. \(2010\)](#) are shown in red, maroon and blue dots, respectively. The known YSO candidates and the comoving sources spatially found to be associated with the *XMM-Newton* X-ray detection are identified using square boxes in magenta. The 4 sources observed by us spectroscopically are identified and marked.

A few of these known YSO candidates show relatively high amount of extinction. In contrast, the majority of the newly identified comoving sources are distributed to the left and lying below the known YSO candidates identified around HD 200775. This suggests that the comoving sources suffer relatively less extinction and exhibit small amount of near-IR excess emission compared to the known YSO candidates. A notable number of them fall in a space between the region occupied by the Class II and Class III (maroon and blue dots, respectively) sources ([Rebull et al. 2010](#)) which indicates that a significant number of them may have some amount of circumstellar material.

The *Spitzer* IRAC (3.6, 4.5, 5.8 and 8.0 μm) flux values given in [Kirk et al. \(2009\)](#) for the known YSO candidates are converted to their respective magnitudes and are shown in the $[3.6]-[4.5]$ vs. $[5.8]-[8.0]$ CC diagram in Fig. 11 using filled circles in green (with reliable *Gaia* DR2 data) and black (without reliable *Gaia* DR2 data). Of the 20 YSO candidates with reliable *Gaia* DR2 data, we obtained *Spitzer* IRAC magnitudes for 15 sources. Of the remaining 38 YSO candidates, 28 are associated with reliable *Spitzer* IRAC magnitudes. Since the IRAC magnitudes for the comoving sources are not available in the literature, we obtained their magnitudes by performing photometry using MOPEX. Nine comoving sources are found to lie outside the *Spitzer* FOV. Four comoving sources do not have reliable photometric flux in 8.0 μm band. None of the comoving sources show emission in MIPS 24 μm . Therefore we show only IRAC magnitudes in Table 6. The remaining seven sources for which we have

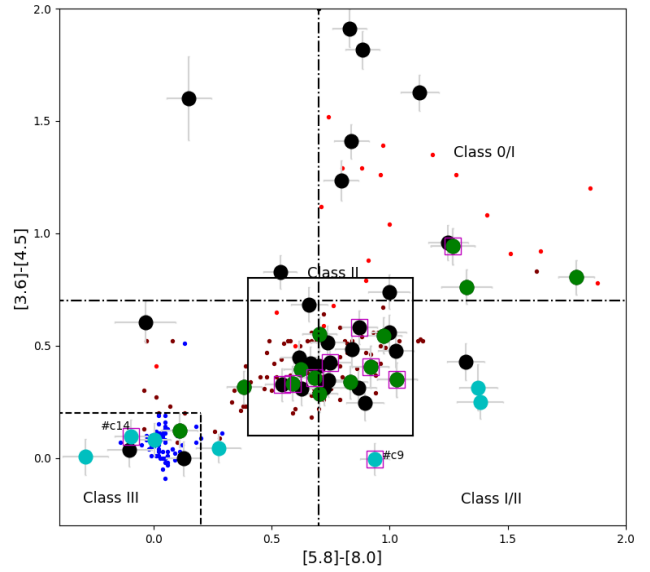


Figure 11. The *Spitzer* CC diagram for the newly identified comoving sources shown using filled cyan circles. The known YSO candidates having reliable *Gaia* data (green circle) and those without reliable *Gaia* data or no detection by the *Gaia* (black circle) are also shown. The Class I, II and III sources taken from [Rebull et al. \(2010\)](#) are shown in red, maroon and blue dots, respectively. The known YSO candidates and the comoving sources spatially found to be associated with the *XMM-Newton* X-ray detection are marked using square boxes in magenta. The 2 sources which are spectroscopically observed by us and have *Spitzer* colours are marked. The boundaries within which Class I, II and III sources generally occupy [Fang et al. \(2009\)](#); [Choudhury et al. \(2010\)](#) are also shown.

reliable data are shown in Fig. 11 using filled circles in cyan. We show the boundaries of Class I, II and III sources adopted from [Fang et al. \(2009\)](#); [Choudhury et al. \(2010\)](#) in Fig. 11. The three new comoving sources are found to occupy the region generally occupied by the Class III sources.

The *WISE* magnitudes for the sources are also obtained from the [Cutri & et al. \(2014\)](#) catalogue by making a search around each of them with a search radius of $3''$. The sources having photometric quality ‘A’ ($\text{SNR} \geq 10$) in $W1$, $W2$ and $W3$ bands are selected as for a majority of the sources, the magnitudes given in the $W4$ band are only upper limits. We confirmed the detection of the sources in each bands by making visual inspection of the *WISE* images in all the bands. We noticed that for a notable number of sources, though the catalogue provides magnitude values in 11.6 and 22.1 μm bands, on visual inspection, no detection was found on the images. The search results are shown in the $[3.4]-[4.6]$ vs. $[4.6]-[11.6]$ CC diagram (Fig. 12). The meaning of the symbols are same as in Fig. 11. Of the 20 comoving sources, we found a counterpart for 7 in the *WISE* database. Among these, one source is common with those shown in Fig. 11. Six additional sources, including #c18, are found in the *WISE* database. Of 20 YSO candidates with reliable *Gaia* DR2 data, we obtained *WISE* magnitudes for 11 sources. Both, the known YSO candidates having reliable *Gaia* DR2 data and the comoving sources are presented in Table 6. Of the remaining known YSO candidates having no reliable data or the *Gaia* detection, we obtained *WISE* magnitudes for

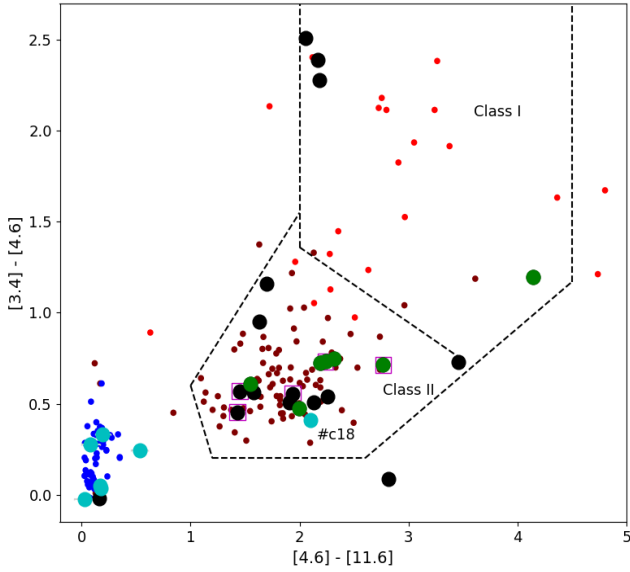


Figure 12. The *WISE* CC diagram for the newly identified comoving sources shown using filled cyan circles. The known YSO candidates detected (green circle) and not detected (black circle) by the *Gaia* are shown using filled circles in green black filled circles. The Class I, II and III sources taken from [Rebull et al. \(2010\)](#) are shown in red, maroon and blue dots respectively. The known YSO candidates and the comoving sources spatially found to be associated with the *XMM-Newton* X-ray detection are marked using square boxes in magenta. The 4 sources observed by us spectroscopically are marked. The dashed lines are the criteria used by [Koenig & Leisawitz \(2014\)](#) to separate the regions occupied by the Class I and Class II sources.

10 sources which are presented in Table 7. In both Fig. 11 and Fig. 12 we again show Class I, II and III (red, maroon and blue dots, respectively) sources taken from [Rebull et al. \(2010\)](#) for comparison.

The difference in the distribution of the known YSO candidates and the comoving sources is more prominent in Fig. 11 and in Fig. 12. It is evident that the known YSO candidates fall in a region generally occupied by Class I and Class II objects. The sources showing spatial association with the X-ray detection are marked with square boxes in magenta. A number of the newly identified comoving sources fall in a region populated by the Class III sources. The comoving source #c18 is located in a region occupied by the Class II sources in *WISE* CC diagram. This is the source which shows second highest $EW(H\alpha)$. The source #c9 which shows a filled-in emission in $H\alpha$ is located in the Class I/II region and the source #c14 which shows smallest $EW(H\alpha)$, occupies Class III region in *Spitzer* CC diagram. The source #c8, which shows highest $EW(H\alpha)$, is not shown in both Fig. 11 and Fig. 12 because of its non-detection by the *Spitzer* IRAC and the *WISE*.

Owing to the lack of reliable photometry in all the bands, we were unable to classify a significant number of comoving sources into various classes based on the CC diagrams. Thus we made an attempt to classify them by calculating their spectral index values. The spectral index, α , is defined as, $\alpha = \frac{d \log F_\lambda}{d \log \lambda}$; where F_λ denotes the flux density at wavelength λ . We calculated the index by a least-squares fit to all the available data from 2MASS K_s ($2.2 \mu\text{m}$) to *WISE*

$22 \mu\text{m}/\text{MIPS } 24 \mu\text{m}$. [Greene et al. \(1994\)](#) proposed the following criteria to classify sources into different evolutionary classes: Class I: $\alpha \geq 0.3$, Flat Spectrum: $0.3 > \alpha \geq -0.3$, Class II: $-0.3 > \alpha \geq -1.6$, and Class III: $\alpha \leq -1.6$. A decrease in the value of α implies that the amount of the circumstellar material around the sources decreases as they evolve. The SEDs and the spectral index values of the “flat” spectrum sources are intermediate between those of deeply embedded “Class I” and those of more evolved Class II YSOs. We obtained spectral index values of the known YSO candidates from [Kirk et al. \(2009\)](#) shown in Table 6 and 7. For five YSO candidates that are not listed in the catalogue by [Kirk et al. \(2009\)](#), we calculated their α values from the available photometric data in various bands. Thus, based on the α values, of the 58 YSO candidates, 7 are classified as Class I, 4 as flat spectrum sources, 35 as Class II and 6 as Class III sources. Of the 20 comoving sources, 4 are classified as Class II and 12 as Class III sources. Remaining 6 YSO candidates and 4 comoving sources are unclassified due to the lack of reliable photometric data.

3.3.4 Optical and near-IR colour-magnitude diagrams

Using G and G_{RP} magnitudes of 20 YSO candidates and 20 comoving sources from the *Gaia* DR2, we constructed M_G vs. $(G-G_{\text{RP}})$ colour-magnitude diagram (CMD). We converted the G magnitudes into absolute magnitudes using the expression $M_G = G + 5 - 5 \log(d)$, where d is the distance taken from [Bailer-Jones et al. \(2018\)](#). Out of 20 YSO candidates for which we have reliable distances from the *Gaia* DR2 (Table 3), extinction values for 11 sources are available in [Kun et al. \(2009\)](#). Based on our spectral type determination, only 4 of the 20 comoving sources have extinction values. As the individual extinction values for most of the sources are unknown, we constructed M_G vs. $(G-G_{\text{RP}})$ CMD without correcting for the extinction. We did not use extinction values provided by the *Gaia* DR2 catalogue as these values are not accurate at the individual star level ([Andrae et al. 2018](#)). The effective temperatures and extinctions listed in *Gaia* DR2 are based on a naked stellar model where the contribution from the dust in the star forming region and/or the protoplanetary disc are ignored.

In Fig. 13 (a) we show the M_G vs. $(G-G_{\text{RP}})$ CMD for the known YSO candidates (filled circles in green) and the newly identified comoving sources (filled circles in cyan) found in the vicinity of HD 200775. The known YSO candidates and the comoving sources that are showing X-ray emission are also marked using magenta square boxes. Also shown are H AeBe ([The et al. 1994](#)), CTTS and WTTS ([Wahhaj et al. 2010](#)) using dots in green, red and blue, respectively. A reddening vector corresponding to a median extinction of 1.6 magnitude estimated by [Kun et al. \(2009\)](#) for NGC 7023 is shown in Fig. 13 (a) and (b). The reddening vector is computed based on [Bossini et al. \(2019\)](#). The PMS isochrones corresponding to 0.1 Myr, 0.5 Myr, 1 Myr and 10 Myr are also shown. We used two grids of models, the CIFIST 2011_2015² models for low mass stars (thick curves in black,

² phoenix.ens-lyon.fr/Grids/BT-Settl/CIFIST2011_2015/ISOCHRONES/

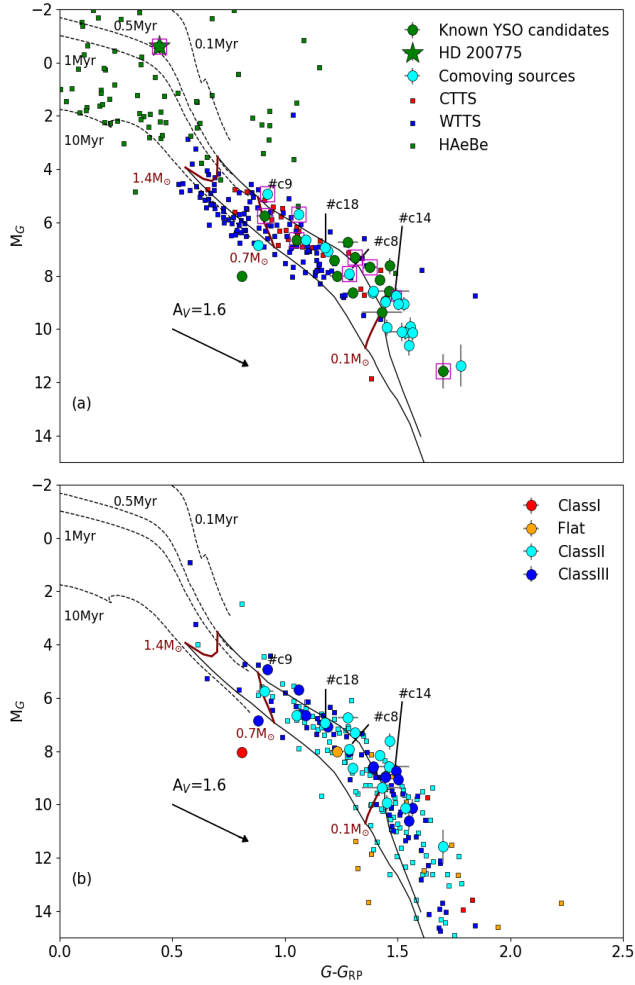


Figure 13. (a) The M_G vs. $(G-G_{RP})$ colour-magnitude plot of the YSO candidates and the comoving sources in the vicinity of HD 200775. The dashed lines indicate the isochrones from PARSEC models (Marigo et al. 2017) and solid curves represent the same from CIFIST models (Baraffe et al. 2015). Green circles: known YSO candidates, cyan circles: newly identified comoving sources, magenta square boxes: X-ray sources. The comoving sources observed spectroscopically are marked. The arrow represents extinction of 1.6 magnitude (the average extinction toward NGC 7023 estimated by Kun et al. 2009). (b) Same as above but the sources are shown according to their classifications. Red square boxes: Class I, orange square boxes: Flat spectrum, cyan square boxes: Class II and blue square boxes: Class III sources.

Baraffe et al. 2015), and the PADOVA tracks Parsec 3.3³ for the higher-mass stars (dashed curves in black, Marigo et al. 2017). Also shown are the positions of HAeBe, CTTS and WTTS sources taken from The et al. (1994) and Wright et al. (2010). The four comoving sources for which we have carried out optical spectroscopy are identified and labeled.

In Fig. 13 (a), a number of known YSO candidates and comoving sources are lying on or above the 1 Myr isochrone. HD 200775 is found to be of ~ 0.5 Myr old which is consistent with the previous studies (Alecian et al. 2008; Vioque et al. 2018; Arun et al. 2019). In Fig. 13 (b) we show M_G

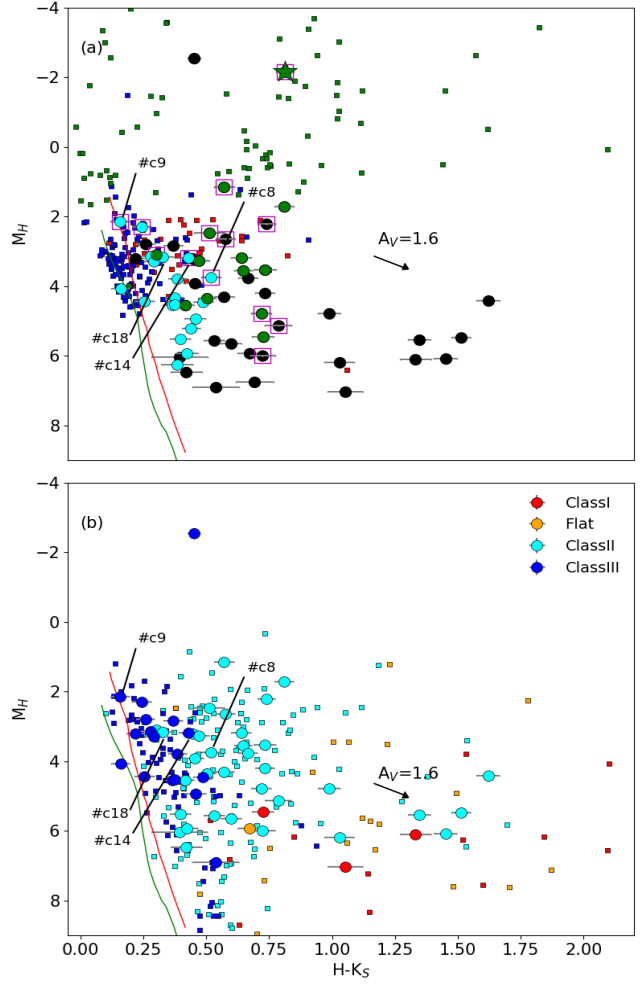


Figure 14. (a) M_H vs. $(H-K_S)$ colour-magnitude plot for sources identified in the vicinity of HD 200775. The PMS isochrones corresponding to 1 Myr (red curve) and 10 Myr (green curve) taken from CIFIST models are drawn. Cyan filled circles: newly identified comoving sources, green filled circles: known YSO candidates having reliable *Gaia* DR2 detection, black filled circles: known YSO candidates without reliable or no *Gaia* DR2 detection, green dots: HAeBe, red dots: CTTS, blue dots: WTTS, green star: HD 200775, magenta square boxes: X-ray sources. The comoving sources observed spectroscopically are marked. (b) Same as above but sources are shown according to their classifications. Red square boxes: Class I, orange square boxes: Flat spectrum, cyan square boxes: Class II and blue square boxes: Class III sources.

vs. $(G-G_{RP})$ CMD of the sources that are classified as Class I, II, III and flat spectrum sources in red, orange, cyan and blue filled circles respectively. Also shown are the locations of Class I, II, III and the flat spectrum sources taken from Rebull et al. (2010), using filled square boxes in red, orange, cyan and blue colors respectively. These are the identified members of the Taurus molecular cloud whose average age is estimated to be ~ 1 Myr (Gomez et al. 1992). A total of 187 out of 257 sources have a *Gaia* DR2 counterpart found within a search radius of $3''$. M_G values of these sources are corrected for their distances obtained from the *Gaia* DR2. All but two sources identified in the vicinity of HD 200775 show a well defined sequence roughly following the 1 Myr isochrone which is consistent with the median age of the

³ stev.oapd.inaf.it/cmd

YSO candidates (~ 1.6 Myr) obtained by Kun et al. (2009). The distribution is found to be similar to the sources found in the Taurus molecular cloud. As the extinction vector is parallel to the isochrones for the sources having $M_G \lesssim 8$ magnitude, the extinction will not affect their distribution. However, for sources having $M_G \gtrsim 8$ magnitude, the effect of extinction can cause erroneous age estimates of the sources as can be noticed in Fig. 13 (b). The source falling below the 10 Myr isochrone is classified by us as a Class I source. This is the only Class I source that shows reliable data in *Gaia* DR2. This source, #15 (Table 3), is identified by Kun et al. (2009) as NGC 7023 RS 10 and they classified it as a variable source. They also found this source to be peculiar as it was showing an age older than 10^8 year. This source is at a distance of 323^{+4}_-5 pc and the proper motion values (7.174 ± 0.079 mas/yr in RA and -1.738 ± 0.075 mas/yr in Dec) are quite consistent with those of other known YSO candidates. As suggested by Kun et al. (2009), this source could be highly variable.

In Fig. 14 (a) and (b) we show M_H vs. $(H-K_S)$ CMD for the sources seen in the vicinity of HD 200775. Considering that a significant number of known YSO candidates and the comoving sources have 2MASS data, it is possible to compare the properties of the comoving and the known YSO candidates including those having no reliable or no *Gaia* DR2 data. The symbols are identical as in Fig. 13 (a) and (b) respectively except that the known YSO candidates without reliable or no *Gaia* DR2 data are shown using filled circles in black. The known YSO candidates and the comoving sources found associated with the X-ray sources are also marked using magenta square boxes. The PMS isochrones corresponding to 1 Myr and 10 Myr taken from the CIFIST models are drawn as red and green curves respectively. A reddening vector corresponding to $A_V=1.6$ magnitude is drawn. In Fig. 14 (a) we also show the HAeBe (The et al. 1994), CTTS and WTTS (Wahhaj et al. 2010) using squares in green, red and blue, respectively. Evidently, the known YSOs having no reliable or no *Gaia* DR2 data are relatively fainter and show higher values of $(H-K_S)$ colors. The faintness of these sources could be because of the extinction suffered by them due to the presence of both interstellar and circumstellar material along the line of sight.

In Fig. 14 (b) we show the sources classified based on their spectral index values. As in Fig. 13 (b), here also we show the Class I, II, III and Flat spectrum sources obtained from Rebull et al. (2010). These sources, associated with the Taurus molecular clouds, show a sequence with the Class I sources lying relatively far away from the 1 Myr isochrone and the Class III sources lying closer to it. The flat spectrum and the Class II sources are found to occupy a region between Class I and Class III sources. Except for the 4 sources that are classified as Class II but showing relatively large $(H-K_S)$ colours, other sources classified as Class I, II, III and Flat spectrum sources in the vicinity of HD 200775 are also found to follow the sequence shown by the YSOs in the Taurus molecular cloud. Of the 55 sources for which we made the classification, we found 3 Class I (5%), 34 Class II (62%), 1 flat spectrum (2%) and 17 Class III (31%) sources towards HD 200775. Based on the classification made by Rebull et al. (2010) for the sources associated with the Taurus molecular cloud, there are 14 Class I (6%), 122 Class II (53%), 20 flat spectrum (8%) and 76 Class III (33%) sources. These are

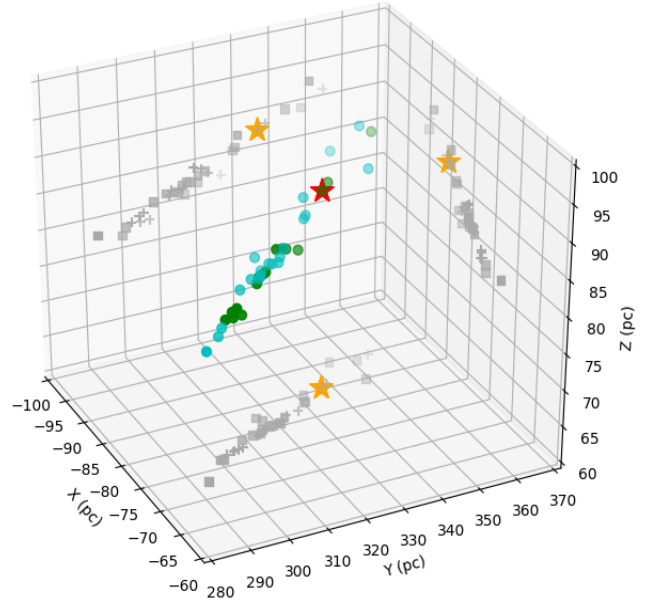


Figure 15. The 3D distribution of the known YSO candidates (filled circles in green) and the comoving (filled circles in cyan) sources having *Gaia* DR2 distances. Their respective projections on the X, Y and Z planes are shown using plus and square symbols in black (X positive towards the Galactic center, Y positive towards the Galactic east and Z positive towards the Galactic north). HD 200775 is identified using a star symbol in red. Its projection in all the three planes is shown using a star in orange.

the 232 sources out of 257, for which we obtained 2MASS counterparts within $3''$ search radius (following the strategy used by Rebull et al. (2010) to get the 2MASS counterparts) and photometric quality of ‘A’ in all the bands. Based on the statistics of the sources found in different categories, it is apparent that the nature of the sources found in the vicinity of HD 200775 and those in the Taurus molecular cloud are very much similar.

3.3.5 Spatial distribution of the sources with respect to HD 200775

Now that the distances to a number of sources towards the direction of HD 200775 are known, we constructed a 3-D distribution of the known YSO candidates and the comoving sources in cartesian coordinate system as shown in Fig. 15. The known YSO candidates and the comoving sources are shown using filled circles in green and cyan, respectively. The projection of the distribution on the X-Y, Y-Z and X-Z planes are also shown (plus sign for the comoving and square boxes for the known YSO candidates). The X-, Y- and Z-positives are towards the Galactic center, the Galactic east and the Galactic north respectively. The location of HD 200775 is shown using a star symbol. We find a significant ($\sim 2\sigma$) shift in the distance of HD 200775 with respect to the distances of other known YSO candidates. Assuming a distance of 335 pc to all the sources (both with and without *Gaia* DR2 data) found in the vicinity of HD 200775, we calculated the projected separation (in parsec) of them with reference to the position of HD 200775. The 2D distribution

of 58 sources (both known YSO candidates and comoving sources having good quality data from 2MASS) thus obtained is shown in Fig. 16. The distribution shows that the maximum projected extent of the sources on the sky plane is ~ 6 pc in diameter. If we assume a similar depth along the line of sight direction also, then HD 200775 will lie outside the cloud. This is inconsistent with the fact that the nebulosity, NGC 7023, is illuminated by HD 200775.

The *Gaia* DR2 distance of 357_{-7}^{+6} pc to HD 200775, though is found to be consistent with the 430_{-90}^{+160} pc estimated using the Hipparcos parallax measurements (van den Ancker et al. 1998), the value is found to be significantly different from the recomputed distance of 520_{-110}^{+180} pc made by van Leeuwen (2007). HD 200775 is a triple system composed of a double-lined spectroscopic binary at ~ 18 mas separation (Millan-Gabet et al. 2001) and a third companion at $6''$ separation (Li et al. 1994). Based on the radial velocity measurements and the astrometric data, Benisty et al. (2013) estimated a dynamical distance of 320 ± 51 pc. We note that binarity was not worked into the astrometric solution for the *Gaia* DR2. The astrometric excess noise (ϵ_i ; Lindegren et al. 2012) which measures the disagreement between the observations of a source and the best-fitting standard astrometric model is found to be 0.185 milli-arcsec for HD 200775. A positive value of ϵ_i signifies that the residuals are statistically larger than expected. The significance of ϵ_i depends on the value of a dimensionless parameter, D (“astrometric_excess_noise_sig”; Lindegren et al. 2012)⁴, which if is greater than 2, implies that ϵ_i is significant. The value of D for HD 200775 is 12.3 suggesting that there is a disagreement between the observations and the standard astrometric model. In addition, the RUWE value of HD 200775 is 1.6, indicating that the astrometric solution is not well-behaved. Presence of unresolved binaries is believed to be one of the reasons for such deviations (Gaia Collaboration et al. 2018a). Therefore the present *Gaia* DR2 parallax measurement of HD 200775 is possibly inaccurate.

In Fig. 16 (a), along the vertical axis we show the ($H-K_S$) colour of the sources considering it to be a proxy for the amount of circumstellar material present around each source. The objects identified as X-ray sources are marked with square boxes in magenta. Evidently, the comoving sources show the lowest of the ($H-K_S$) colour and are spatially well correlated with the known YSO candidates. A majority of the sources (44 or 75%) are distributed within ~ 1 pc distance from HD 200775, 8 ($\sim 13\%$) are distributed between 1 and 2 pc and only 7 ($\sim 12\%$) are located beyond 2 pc. Both the known YSO candidates and the comoving sources are among the sources distributed within 1 pc from HD 200775. The distribution of the sources presented in Fig. 16 shows an enhancement in the vicinity of HD 200775 but, instead of a high density clustering, we detect a loose association. Dynamical dissipation was suggested as one of the possible reasons for the lack of clustering in HD 200775 (Fuente et al. 2001). The distribution of the proper motions of the young stars associated with a region can yield the velocity dispersion provided the distance is well known. Using the distance of 335 pc and the dispersion in the proper motion

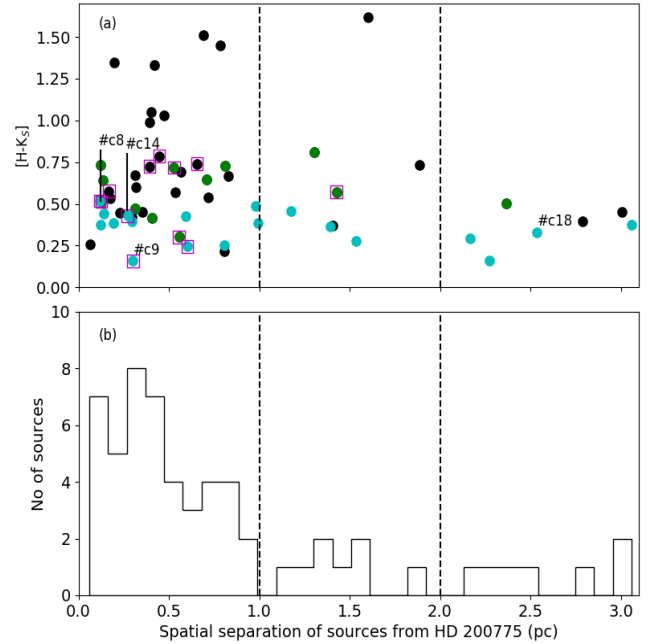


Figure 16. (a) The 2D spatial distribution of the known YSO candidates (filled circles in green: sources having reliable *Gaia* data, filled circles in black: sources without *Gaia* data) and the newly identified comoving sources (filled circles in cyan) with respect to the star HD 200775. Their ($H-K_S$) values are shown in the vertical axis. Sources having X-ray emission are marked with magenta square boxes. The sources observed by us using HFOSC are also marked. (b) Histogram of the distribution of the known YSO candidates and the newly identified comoving sources with respect to the star HD 200775.

values in RA and Dec for the known YSO candidates and the comoving sources combined, we calculated a velocity dispersion of ~ 1 km s⁻¹ for the sources found in the vicinity of HD 200775. Given the velocity dispersion and an age of ~ 1 Myr, the sources around HD 200775 could have moved by ~ 1 pc from where they were born. If we assume that they were all born very close to HD 200775, the distribution seen in Fig. 16 is quite consistent. But in such a case, we expect the distribution of the known YSO candidates and the comoving sources around HD 200775 to be symmetrical.

In Fig. 17 (a) we show the distribution of 59 sources (YSO candidates + comoving sources) that fall within the *Herschel* dust column density map. The known YSO candidates are identified using red square symbols. Of these, the sources having no reliable *Gaia* DR2 data are identified with red square + white dot. The comoving sources are shown using circles in yellow. Both the known YSO candidates and the comoving sources associated with the X-ray detection are identified using cross symbols. The contours shown in thick lines represent the source distribution around HD 200775 (white star symbol). The distribution of the sources is not symmetrical with respect to HD 200775. At immediate surroundings of HD 200775, source distribution is concentrated more towards the north and as we move further out, sources are sparsely distributed more in the east-west direction. Testi et al. (1999) found a correlation between the spectral type of HAeBe stars and the stellar density surrounding

⁴ https://gea.esac.esa.int/archive/documentation/GDR2/Gaia_archive/chap_datamodel/

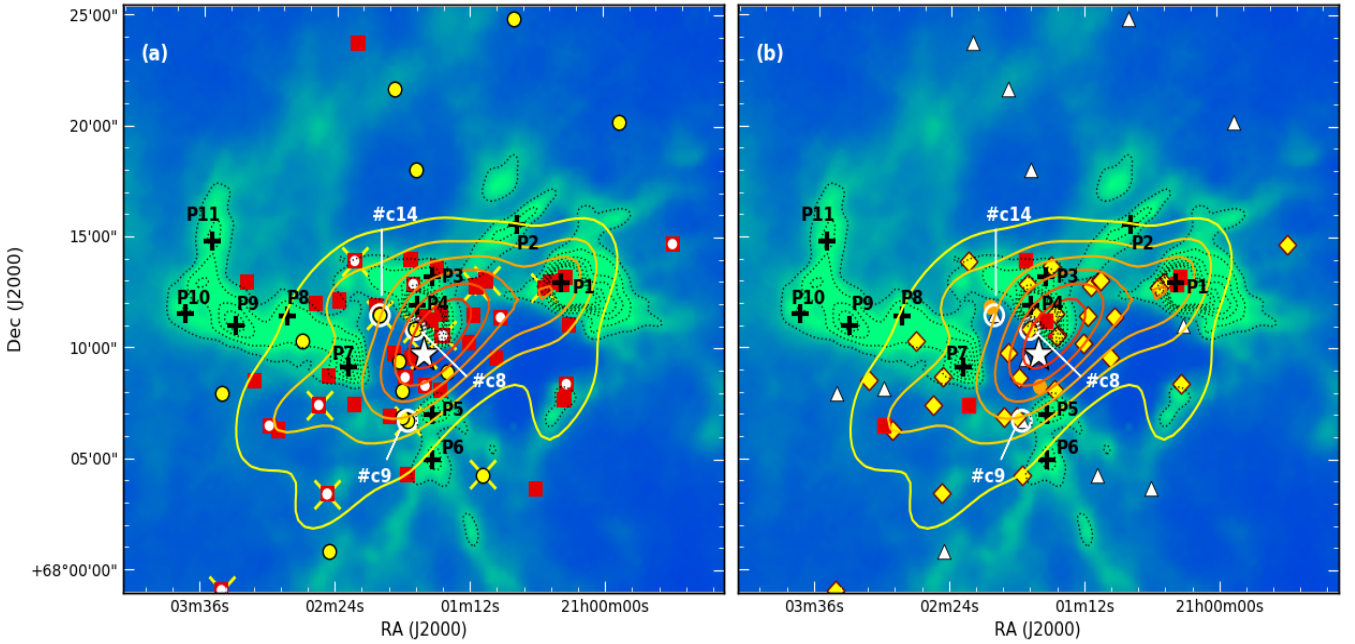


Figure 17. (a) The spatial distribution of the YSO candidates and the comoving sources overplotted on the *Herschel* column density map of the region surrounding HD 200775. The position of HD 200775 is identified using a white star symbol. Peak emission regions are shown in black ‘+’ symbols. Red square: known YSO candidates; Red square + white dot: known YSO candidates with reliable *Gaia* DR2 data; Yellow filled circle: comoving sources identified in this work; Yellow filled circle + open circle in white: comoving sources observed by us spectroscopically; Yellow cross: X-ray detection by the *XMM-Newton* satellite. Black Plus: Column density peaks. The contours shown in thick lines represent the source distribution around HD 200775. (b) Represents the same as (a) but with the classifications of the sources. Red square box: Class I, Orange filled circle: Flat spectrum, Yellow diamond: Class II, White filled triangle: Class III sources.

them. However, HD 200775 was shown as an exception due to the lack of clustering around it. [Testi et al. \(2001\)](#) discussed the results in connection with two competing models, namely, physical ([Bonnell et al. 1998](#)) and random sampling models ([Elmegreen 1999](#)) which are advocated to explain the formation of high-mass stars. According to the physical models, the presence of clustering is a pre-requisite for the formation of massive stars but on the other hand, they are unrelated according to the random models. In fact, the presence of a few of the massive stars (like HD 200775) not surrounded by an enhanced stellar density was shown as a support to the random models. Even with the identification of 20 additional comoving sources in the vicinity of HD 200775, because these sources are more sparsely distributed compared to the known YSO candidates, the stellar density around HD 200775 is still very low and hence favours the random sampling models.

HD 200775 is residing inside a biconical cavity, which is believed to have been carved out in an earlier evolutionary stage by a currently inactive bipolar outflow ([Fuente et al. 1996](#)). The outflow axis runs along the east-west direction. [Fuente et al. \(1998a\)](#), based on the morphology of the parent cloud, classified H A e Be stars into three groups. They classified HD 200775 as Type III which implies that the source has completely dispersed the surrounding dense gas and is currently located inside a cavity of molecular cloud. The expulsion of gas from the vicinity of OB stars could limit the amount of molecular material available for the formation of additional stars which could be a possible reason for the lack

of clustering around HD 200775. Using the CLUMPFIND ([Williams et al. 1994](#)) task on the dust column density map made using the *Herschel* images, we found a total of 11 peak emission regions (P1 - P11) which are shown in Fig. 17. The contours are plotted from 3.2×10^{21} to 1.1×10^{22} cm^{-2} in steps of 1.3×10^{21} cm^{-2} . While two peak emission regions are located to the north and two to the south of HD 200775, the rest of the peaks are distributed mostly along the east-west direction. This roughly coincides with the orientation of the biconical cavity ([Fuente et al. 1996](#)). The velocity-intensity map of ^{13}CO J=2-1 gas emission ([Yuan et al. 2013](#)) and the dust emission (Fig. 17) surrounding HD 200775 show a large intensity gradient along the sides facing HD 200775. It is possible that the bipolar outflow and the stellar wind from HD 200775 might have been responsible for shaping the geometry of the material seen around it.

A significant number of the sources are found to be associated with the peaks towards P1, P3 and P4. Evidence of current star formation is seen towards P1 (e.g., [Rector & Schweiker 2013](#)). Using ^{12}CO J=3-2 observations, [Yuan et al. \(2013\)](#) detected a non-Gaussian line profile with the peak skewed to the blue indicative of infall motions. Presence of infall motions suggests that star formation is still active. In Fig. 17 (b), we show the distribution of sources classified as Class I, II, III and flat spectrum sources. Of the six sources classified as Class I, five (squares in red) are located within the mapped area. Among these, three sources are located towards P1 and P4. Possibly, star formation in L1172/1174 complex might have begun roughly ~ 1 Myr ago but the

very young sources, particularly those of Class I type, which are associated with the P1 and P4 peaks might have been formed as a result of positive feedback from HD 200775. P1 is found to be associated with two Class I sources and a number of outflows (Kirk et al. 2009; Rector & Schweiker 2013). A dynamical age of ~ 7500 yr is estimated by Rector & Schweiker (2013). This suggests that some of these young sources might have been formed very recently. The presence of infall motions in Core 1 (P1 in Fig. 17) and intensity gradient to the south of Core 3 (P3 and P4 in Fig. 17) shown by Yuan et al. (2013) supports this argument. Based on this and the shock features observed at $4.5\mu\text{m}$, they suggested that star formation around HD 200775 could have been possibly triggered due to HD 200775. Star formation scenario in the Cepheus region was presented by Kun et al. (2009). However, to understand the history of star formation, it is important to study the true nature of the rest of the comoving sources and study the dynamical state of the gas surrounding HD200775.

4 CONCLUSIONS

The region surrounding the well-known reflection nebula, NGC 7023, illuminated by a Herbig Be star, HD 200775, located in the dark cloud L1174 is known for low to intermediate-mass star formation activity. Distance to L1172/1174 complex of which L1174 is a part is not very well constrained. In this work, using *Gaia* DR2 distances and proper motion values, we determined distance to the cloud using the known YSO candidates. We also used polarization measurements of 545 stars that are projected on the cloud to estimate the same. Then we searched for additional comoving sources in the vicinity of HD 200775. The main results from this study are summarized below:

- Based on the distances and proper motion values of 20 previously known YSO candidates associated with L1174 we obtained a distance of 335 ± 11 pc to the cloud. The distance estimated for the entire cloud using the polarization measurements of the foreground and background stars was also found to be consistent with the ~ 335 pc distance.

- With the knowledge of distance and proper motion values of the YSO candidates associated with the cloud, we searched for additional comoving sources in the vicinity ($1^\circ \times 1^\circ$ area) of HD 200775. We found a total of 20 sources which are comoving with the known YSO candidates. Compared to the known YSO candidates, the comoving sources are found to show less IR excess. From their locations on the CMDs (optical and near-IR) and by comparison with the PMS isochrone models, they are found to be young (~ 1 Myr) sources.

- Based on the *XMM-Newton* data, we found 19 reliable X-ray detection around HD200775. Of these, 10 are found to be associated with the known YSO candidates and 4 with the newly identified comoving sources.

- We made spectroscopic observations of 4 of the 20 comoving sources of which three are X-ray sources. We found $H\alpha$ in emission in 3 of the 4 sources.

- We classified the YSO candidates and the comoving sources based on their spectral index values as Class I, II, III and flat spectrum sources. A majority of the comoving sources are classified as Class III. About 80% of the known

YSO candidates and the comoving sources are found to be distributed within ~ 1 pc distance from HD 200775.

- Spatial correlation of a number of Class I sources with the density peaks of dust identified from the *Herschel* map suggests that star formation is currently active in the vicinity of HD 200775 and some of these young sources could have been formed as a result of positive feedback from it.

A detailed study of all the identified sources, especially, the 20 newly identified comoving sources is required to estimate their spectral type, extinction and luminosity to confirm their true characteristics.

ACKNOWLEDGEMENTS

We thank all the supporting staff at ARIES, Nainital and the staff of IAO, Hanle and CREST, Hosakote, who made these observations possible. The facilities at IAO and CREST are operated by the Indian Institute of Astrophysics, Bangalore. C.W.L was supported by the Basic Science Research Program (2019R1A2C1010851) through the National Research Foundation of Korea. This work has made use of data from the following sources: (1) European Space Agency (ESA) mission *Gaia* (<https://www.cosmos.esa.int/gaia>), processed by the *Gaia* Data Processing and Analysis Consortium (DPAC, <https://www.cosmos.esa.int/web/gaia/dpac/consortium>). Funding for the DPAC has been provided by national institutions, in particular the institutions participating in the *Gaia* Multilateral Agreement; (2) the Two Micron All Sky Survey, which is a joint project of the University of Massachusetts and the Infrared Processing and Analysis Center/California Institute of Technology, funded by the National Aeronautics and Space Administration and the National Science Foundation; (3) the *Herschel* SPIRE images from *Herschel* Science Archive (HSA). *Herschel* is an ESA space observatory with science instruments provided by European-led Principal Investigator consortia and with important participation from NASA; (4) the NASA/IPAC Infrared Science Archive, which is operated by the Jet Propulsion Laboratory, California Institute of Technology, under contract with the National Aeronautics and Space Administration; (5) the Wide-field Infrared Survey Explorer, which is a joint project of the University of California, Los Angeles, and the Jet Propulsion Laboratory/California Institute of Technology, funded by the National Aeronautics and Space Administration; (6) the *XMM-Newton*, an ESA science mission with instruments and contributions directly funded by ESA Member States and NASA; and (7) the SIMBAD database is operated at CDS, Strasbourg, France.

REFERENCES

- Alecian E., et al., 2008, *MNRAS*, **385**, 391
 Alves F. O., Franco G. A. P., 2007, *A&A*, **470**, 597
 Andrae R., et al., 2018, *A&A*, **616**, A8
 Andre P., Ward-Thompson D., Barsony M., 1993, *ApJ*, **406**, 122
 Appenzeller I., Mundt R., 1989, *A&ARv*, **1**, 291
 Armandroff T. E., Herbst W., 1981, *AJ*, **86**, 1923
 Arun R., Mathew B., Manoj P., Ujjwal K., Kartha S. S., Viswanath G., Narang M., Paul K. T., 2019, *AJ*, **157**, 159
 Bailer-Jones C. A. L., 2015, *PASP*, **127**, 994

- Bailer-Jones C. A. L., Rybizki J., Fousneau M., Mantelet G., Andrae R., 2018, *AJ*, **156**, 58
- Baraffe I., Homeier D., Allard F., Chabrier G., 2015, *A&A*, **577**, A42
- Barcons X., et al., 2007, *A&A*, **476**, 1191
- Barrado y Navascués D., Martín E. L., 2003, *AJ*, **126**, 2997
- Benisty M., et al., 2013, *A&A*, **555**, A113
- Bonnell I. A., Bate M. R., Zinnecker H., 1998, *MNRAS*, **298**, 93
- Bossini D., et al., 2019, *A&A*, **623**, A108
- Choudhury R., Mookerjee B., Bhatt H. C., 2010, *ApJ*, **717**, 1067
- Clemens D. P., Yun J. L., Heyer M. H., 1991, *ApJS*, **75**, 877
- Crutcher R. M., 2012, *ARA&A*, **50**, 29
- Cutri R. M., et al. 2014, VizieR Online Data Catalog, **2328**
- Cutri R. M., et al., 2003, VizieR Online Data Catalog, **2246**
- Davis Jr. L., Greenstein J. L., 1951, *ApJ*, **114**, 206
- Dzib S. A., Loinard L., Ortiz-León G. N., Rodríguez L. F., Galli P. A. B., 2018, *ApJ*, **867**, 151
- Elmegreen B. G., 1999, *ApJ*, **515**, 323
- Elmegreen D. M., Elmegreen B. G., 1978, *ApJ*, **220**, 510
- Evans Neal J. I., et al., 2009, *ApJS*, **181**, 321
- Faherty J. K., Bochanski J. J., Gagné J., Nelson O., Coker K., Smithka I., Desir D., Vasquez C., 2018, *ApJ*, **863**, 91
- Fang M., van Boekel R., Wang W., Carmona A., Sicilia-Aguilar A., Henning T., 2009, *A&A*, **504**, 461
- Fuente A., Martín-Pintado J., Neri R., Rogers C., Moriarty-Schieven G., 1996, *A&A*, **310**, 286
- Fuente A., Martín-Pintado J., Bachiller R., Neri R., Palla F., 1998a, *A&A*, **334**, 253
- Fuente A., Martín-Pintado J., Rodríguez-Franco A., Moriarty-Schieven G. D., 1998b, *A&A*, **339**, 575
- Fuente A., Neri R., Martín-Pintado J., Bachiller R., Rodríguez-Franco A., Palla F., 2001, *A&A*, **366**, 873
- Gaia Collaboration et al., 2018a, *A&A*, **616**, A1
- Gaia Collaboration et al., 2018b, *A&A*, **616**, A10
- Getman K. V., et al., 2011, *ApJS*, **194**, 3
- Gomez M., Jones B. F., Hartmann L., Kenyon S. J., Stauffer J. R., Hewett R., Reid I. N., 1992, *AJ*, **104**, 762
- Greene T. P., Wilking B. A., Andre P., Young E. T., Lada C. J., 1994, *ApJ*, **434**, 614
- Grenier I. A., Lebrun F., Arnaud M., Dame T. M., Thaddeus P., 1989, *ApJ*, **347**, 231
- Heiles C., 1967, *ApJS*, **15**, 97
- Heiles C., 2000, *AJ*, **119**, 923
- Heyer M., Dame T. M., 2015, *ARA&A*, **53**, 583
- Hilton J., Lahulla J. F., 1995, *A&AS*, **113**, 325
- Jacoby G. H., Hunter D. A., Christian C. A., 1984, *ApJS*, **56**, 257
- Kauffmann J., Bertoldi F., Bourke T. L., Evans II N. J., Lee C. W., 2008, *A&A*, **487**, 993
- Kirk J. M., et al., 2009, *ApJS*, **185**, 198
- Knude J., Hog E., 1998, *A&A*, **338**, 897
- Koenig X. P., Leisawitz D. T., 2014, *ApJ*, **791**, 131
- Kun M., 1998, *ApJS*, **115**, 59
- Kun M., Kiss Z. T., Balog Z., 2008, Star Forming Regions in Cepheus. p. 136
- Kun M., Balog Z., Kenyon S. J., Mamajek E. E., Gutermuth R. A., 2009, *ApJS*, **185**, 451
- Lada C. J., 1987, in Peimbert M., Jugaku J., eds, IAU Symposium Vol. 115, Star Forming Regions. pp 1–17
- Li W., Evans II N. J., Harvey P. M., Colome C., 1994, *ApJ*, **433**, 199
- Lindgren L., 2018, Re-normalising the astrometric chi-square in Gaia DR2, GAIA-C3-TN-LU-LL-124, http://www.rssd.esa.int/doc_fetch.php?id=3757412
- Lindgren L., Lammers U., Hobbs D., O’Mullane W., Bastian U., Hernández J., 2012, *A&A*, **538**, A78
- López-Santiago J., Caballero J. A., 2008, *A&A*, **491**, 961
- Luhman K. L., 2018, *AJ*, **156**, 271
- Luhman K. L., Herrmann K. A., Mamajek E. E., Esplin T. L., Pecaut M. J., 2018, *AJ*, **156**, 76
- Lynds B. T., 1962, *ApJS*, **7**, 1
- Maheswar G., Lee C. W., Bhatt H. C., Mallik S. V., Dib S., 2010, *A&A*, **509**, A44
- Makovoz D., Marleau F. R., 2005, *PASP*, **117**, 1113
- Manoj P., Bhatt H. C., Maheswar G., Muneer S., 2006, *ApJ*, **653**, 657
- Marigo P., et al., 2017, *ApJ*, **835**, 77
- McClure M. K., et al., 2010, *ApJS*, **188**, 75
- Millan-Gabet R., Schloerb F. P., Traub W. A., 2001, *ApJ*, **546**, 358
- Nazé Y., Petit V., Rinbrand M., Cohen D., Owocki S., ud-Doula A., Wade G. A., 2014, *ApJS*, **215**, 10
- Ramaprakash A. N., Gupta R., Sen A. K., Tandon S. N., 1998, *A&AS*, **128**, 369
- Rautela B. S., Joshi G. C., Pandey J. C., 2004, Bulletin of the Astronomical Society of India, **32**, 159
- Rebull L. M., et al., 2010, *ApJS*, **186**, 259
- Rector T. A., Schweiker H., 2013, *AJ*, **145**, 35
- Reed B. C., 2000, *AJ*, **120**, 314
- Robitaille T. P., Whitney B. A., Indebetouw R., Wood K., 2007, *ApJS*, **169**, 328
- Romano G., 1975, *Ap&SS*, **33**, 487
- Rosen S. R., et al., 2016, *A&A*, **590**, A1
- Schmidt G. D., Elston R., Lupie O. L., 1992, *AJ*, **104**, 1563
- Shevchenko V. S., Ibragimov M. A., Yakubov S. D., 1989, *Soviet Ast.*, **33**, 487
- Soam A., Maheswar G., Bhatt H. C., Lee C. W., Ramaprakash A. N., 2013, *MNRAS*, **432**, 1502
- Soam A., Maheswar G., Lee C. W., Dib S., Bhatt H. C., Tamura M., Kim G., 2015, *A&A*, **573**, A34
- Soam A., Maheswar G., Lee C. W., Neha S., Andersson B.-G., 2017, *MNRAS*, **465**, 559
- Straizys V., Cernis K., Kazlauskas A., Meistas E., 1992, *Baltic Astronomy*, **1**, 149
- Testi L., Palla F., Natta A., 1999, *A&A*, **342**, 515
- Testi L., Palla F., Natta A., 2001, The Onset of Cluster Formation Around Intermediate-Mass Stars. p. 377
- The P. S., de Winter D., Perez M. R., 1994, *A&AS*, **104**, 315
- Vioque M., Oudmaijer R. D., Baines D., Mendigutía I., Pérez-Martínez R., 2018, *A&A*, **620**, A128
- Viotti R., 1969, *Mem. Soc. Astron. Italiana*, **40**, 75
- Wahhaj Z., et al., 2010, *ApJ*, **724**, 835
- Weston E. B., 1953, *AJ*, **58**, 48
- Whittet D. C. B., Prusti T., Franco G. A. P., Gerakines P. A., Kilkenny D., Larson K. A., Wesselius P. R., 1997, *A&A*, **327**, 1194
- Williams J. P., de Geus E. J., Blitz L., 1994, *ApJ*, **428**, 693
- Wright E. L., et al., 2010, *AJ*, **140**, 1868
- Yuan J.-H., Wu Y., Li J. Z., Yu W., Miller M., 2013, *MNRAS*, **429**, 954
- Yun J. L., Clemens D. P., 1990, *ApJ*, **365**, L73
- Zdanavičius K., Zdanavičius J., Straizys V., Maskoliūnas M., 2009, *Baltic Astronomy*, **18**, 33
- van Leeuwen F., 2007, *A&A*, **474**, 653
- van den Ancker M. E., de Winter D., Tjin A Djie H. R. E., 1998, *A&A*, **330**, 145

Table 3. Distance and proper motion values of the known YSO candidates identified towards L1172/1174 from *Gaia* DR2.

#	RA (°)	Dec (°)	Source ID	Distance (pc)	μ_{α^*} ($\Delta\mu_{\alpha^*}$) (mas/yr)	μ_{δ} ($\Delta\mu_{\delta}$) (mas/yr)	G (eG) (mag)	RUWE	Spectral Type	H α EW(Å)	2MASS	<i>Spitzer</i>	<i>WISE</i>	X-ray
(1)	(2)	(3)	(4)	(5)	(6)	(7)	(8)	(9)	(10)	(11)	(12)	(13)	(14)	(15)
1	314.845315	68.245467	2270256357606156160	339 $^{+5}_{-5}$	7.333±0.087	-1.599±0.079	14.3789±0.0150	1.1	K1	-9.6	✓	✓	✓	✓
2	315.084447	68.140772	2270240208529136128	341 $^{+10}_{-10}$	7.630±0.147	-1.182±0.158	17.0301±0.0309	1.1	-	-	✓	✓	✓	✓
3	315.231481	68.190885	2270240723925216640	333 $^{+12}_{-13}$	7.205±0.184	-1.649±0.280	16.5545±0.0020	1.3	-	-	✓	✓	✓	✓
4	315.359984	68.177338	2270245637367812352	325 $^{+7}_{-6}$	7.652±0.104	-1.416±0.121	14.8691±0.0049	1.2	M0IV	-59.8	✓	✓	✓	✓
5	315.362884	68.177214	2270245637367812608	360 $^{+13}_{-13}$	6.667±0.174	-0.865±0.189	16.3712±0.0266	1.5	M0	-63.9	✓	-	-	-
6*	315.399160	68.223752	2270246874315480960	277 $^{+27}_{-34}$	11.343±0.673	-3.039±0.706	17.7558±0.0107	3.3	-	-	✓	✓	✓	-
7	315.400352	68.139576	2270245259410695808	332 $^{+9}_{-6}$	6.971±0.106	-1.638±0.117	15.6235±0.0130	1.4	M0	-106.0	-	✓	✓	-
8	315.403923	68.163263	2270245431209611776	357 $^{+6}_{-5}$	8.336±0.079	-1.566±0.083	7.1592±0.0010	1.6	-	-	✓	-	-	✓
9	315.427117	68.215960	2270246148467658624	323 $^{+8}_{-9}$	7.530±0.148	-0.668±0.164	15.6942±0.0033	1.5	M2	-28.8	✓	✓	✓	-
10	315.444875	68.145894	2270057689598399360	335 $^{+5}_{-4}$	7.770±0.071	-1.428±0.078	15.0363±0.0057	1.1	M1	-64.5	✓	✓	-	-
11	315.558650	68.233141	2270247492790812928	321 $^{+26}_{-31}$	8.666±0.528	-1.736±0.568	19.1129±0.0059	1.1	-	-	✓	✓	✓	✓
12*	315.584979	68.423341	2270276041439733504	277 $^{+19}_{-22}$	7.262±0.483	-3.589±0.530	14.6337±0.0158	7.9	-	-	✓	-	✓	-
13	315.617758	68.058287	2270056246489398528	343 $^{+9}_{-6}$	6.868±0.098	-1.319±0.107	15.3618±0.0053	1.1	K7	-56.0	-	✓	✓	✓
13b	315.618244	68.057669	2270056246489398400	376 $^{+16}_{-15}$	8.041±0.193	-1.202±0.215	15.5062±0.0010	1.5	M4.5IV	-7.5	-	-	-	-
14	315.637634	68.124746	2270056968043900928	336 $^{+3}_{-2}$	7.054±0.044	-1.017±0.043	14.2794±0.0078	1.0	K5	-4.0	✓	✓	✓	✓
15	315.747855	68.108939	2270053875667453056	323 $^{+4}_{-5}$	7.174±0.079	-1.738±0.075	15.5766±0.0061	1.5	K4	-8.1	✓	✓	✓	-
16*	315.748555	68.136623	2270058303777440640	401 $^{+85}_{-149}$	5.678±0.849	-11.026±1.196	16.5831±0.0108	4.7	-	-	✓	✓	✓	-
17	315.851719	67.985134	2270052256462948736	326 $^{+8}_{-8}$	7.269±0.140	-2.330±0.128	13.3182±0.0111	5.9	K2	-13.1	✓	✓	✓	✓
18*	315.923249	68.396018	2270272330587968256	559 $^{+28}_{-230}$	5.407±0.780	-3.269±0.752	17.4905±0.0045	4.1	-	-	✓	-	✓	-
19	315.997585	67.824847	2270035287049455616	346 $^{+8}_{-9}$	7.722±0.152	-2.061±0.133	16.3326±0.0041	1.4	-	-	✓	✓	✓	-

Columns 2 & 3: 2015.5 epoch Right Ascension & Declination of sources given by *Gaia* DR2.

Column 4: Distance taken from the [Bailer-Jones et al. \(2018\)](#) catalogue.

Column 9: Renormalised Unit Weight Error (RUWE) of the YSO candidates.

Columns 10 & 11: Spectral type and equivalent width of H α taken from [Kun et al. \(2009\)](#).

Column 13: X-ray detection by *XMM-Newton*.

Stars #4 & #5 appear as double sources. Resolved by *Gaia* DR2, 2MASS and *Spitzer*. In *WISE* and *XMM-Newton*, they are detected as single source. *WISE* and X-ray are assigned to the brightest source in K_s band.

Stars #13 & #13b appear as double sources. Resolved only by *Gaia* DR2. 2MASS classified it as an extended source. Assigned X-ray detection to the brightest source in *Gaia*.

* Sources considered as outliers in our analysis.

Table 4. Distance and proper motion values of the comoving sources from *Gaia* DR2.

#	RA(2015.5) (°)	Dec(2015.5) (°)	Source ID	Distance (pc)	$\mu_{\alpha\star}$ ($\Delta\mu_{\alpha\star}$) (mas/yr)	μ_{δ} ($\Delta\mu_{\delta}$) (mas/yr)	G (eG) (mag)	RUWE	Spectral Type	H α EW (Å)	2MASS	<i>Spitzer</i>	<i>WISE</i>	X-ray	Spectral Index α
(1)	(2)	(3)	(4)	(5)	(6)	(7)	(8)	(9)	(10)	(11)	(12)	(13)	(14)	(15)	(16)
c1	314.358914	68.184721	2270164445306098560	311 ³ ₋₂	6.372±0.066	-3.263±0.041	14.321±0.000	1.0	-	-	✓	-	✓	-	-2.78
c2	314.877400	67.678993	2269947738436093696	369 ¹³ ₋₁₃	7.472±0.183	-3.129±0.216	16.881±0.002	1.0	-	-	✓	-	✓	-	-2.41
c3	314.963955	68.336928	2270263092114875520	373 ¹³ ₋₁₃	7.315±0.177	-1.844±0.166	16.825±0.002	1.0	-	-	✓	-	✓	-	-2.56
c4	315.201051	68.415148	2270265016260228608	352 ⁵ ₋₅	7.073±0.074	-0.752±0.079	14.800±0.001	1.1	-	-	✓	-	✓	-	-2.66
c5	315.271845	68.072754	2270238795483033728	340 ³ ₋₃	7.294±0.048	-1.576±0.056	13.363±0.006	1.2	-	-	✓	-	✓	✓	-2.52
c6	315.350786	68.150243	2270245289474206848	351 ¹⁷ ₋₁₆	8.195±0.233	-0.846±0.271	17.622±0.003	1.3	-	-	✓	-	-	-	-
c7	315.420625	68.301379	2270248798463735808	331 ⁹ ₋₈	7.510±0.142	-1.452±0.170	16.243±0.001	1.2	-	-	✓	✓	✓	✓	-2.32
c8	315.422157	68.182326	2270245465569124608	337 ⁶ ₋₆	7.222±0.096	-1.154±0.105	15.564±0.002	1.3	M1	-15.03	✓	-	✓	✓	-0.73
c9	315.439309	68.113265	2270057483439969408	342 ² ₋₃	7.595±0.042	-3.004±0.046	12.600±0.002	1.0	K2	-0.69	✓	✓	✓	✓	-2.45
c10	315.450292	68.115938	2270057517799708032	338 ¹³ ₋₁₃	8.084±0.206	-1.537±0.280	17.776±0.002	1.0	-	-	✓	✓	✓	-	-0.61
c11	315.452017	68.135740	2270057685302330240	350 ⁴³ ₋₃₄	8.426±0.623	-2.081±0.684	19.088±0.004	1.3	-	-	✓	-	-	-	-
c12	315.458232	68.158415	2270057723958137600	333 ¹³ ₋₁₂	8.312±0.202	-1.153±0.219	16.674±0.001	1.5	-	-	✓	-	-	-	-
c13	315.470563	68.362746	2270252367579936768	328 ¹⁸ ₋₁₇	8.544±0.324	-1.593±0.369	18.204±0.002	1.1	-	-	✓	✓	✓	-	-2.30
c14	315.501565	68.192440	2270245809166510080	319 ¹¹ ₋₁₀	7.975±0.177	-1.400±0.193	16.260±0.001	1.3	M3	-4.06	✓	✓	✓	✓	-1.98
c15	315.612647	68.015216	2270053081097108480	339 ¹⁷ ₋₁₄	7.643±0.282	-1.804±0.294	17.782±0.002	1.0	-	-	✓	-	✓	-	-2.21
c16	315.675742	68.172632	2270058651671079808	334 ¹⁵ ₋₁₃	7.885±0.231	-1.042±0.250	17.566±0.005	1.3	-	-	✓	✓	✓	-	-1.45
c17	315.853497	68.132781	2270055421855682688	318 ⁸ ₋₈	7.334±0.146	-1.539±0.137	16.103±0.002	1.2	-	-	✓	✓	✓	-	-2.39
c18	316.150453	68.498418	2270280409423293952	336 ⁵ ₋₅	7.372±0.078	-1.308±0.068	14.571±0.004	1.4	M1	-13.01	✓	-	✓	-	-0.80
c19	316.151474	68.496975	2270280405127009024	366 ¹⁹ ₋₁₇	7.148±0.242	-1.375±0.237	17.925±0.017	1.0	-	-	-	-	-	-	-
c20	316.394054	68.209051	2270068512916332672	336 ³ ₋₃	8.417±0.054	-1.372±0.053	14.290±0.003	1.2	-	-	✓	-	✓	-	-2.67

Columns 2 & 3: 2015.5 epoch Right Ascension & Declination of sources given by *Gaia* DR2.

Column 4: Distance taken from the [Bailer-Jones et al. \(2018\)](#) catalogue.

Column 9: Renormalised Unit Weight Error (RUWE) of the comoving sources.

Column 15: X-ray detection by *XMM-Newton*.

Table 5. X-ray sources detected by *XMM-Newton* around HD 200775.

#	RA (2000) (°)	Dec (2000) (°)	r (")	HR1	e_HR1	HR2	e_HR2	2MASS	<i>Spitzer</i>	<i>WISE</i>
X-ray sources associated with the known YSO candidates										
4	315.360137	68.177384	0.346	0.96	0.04	0.30	0.05	✓	✓	✓
8	315.403845	68.163229	0.079	0.85	0.01	0.30	0.01	✓	-	-
11	315.558856	68.232957	0.973	0.97	0.65	0.93	0.09	✓	✓	✓
13 [†]	315.617351	68.058043	0.723	0.79	0.15	0.24	0.14	-	✓	✓
14	315.637078	68.124783	0.561	0.72	0.06	-0.10	0.06	✓	✓	✓
17	315.849525	67.984878	2.996	0.92	0.08	0.31	0.10	✓	✓	✓
27	315.133771	68.213195	0.324	1.00	0.04	0.73	0.03	✓	✓	✓
30	315.261981	68.218805	0.728	0.94	0.17	0.47	0.13	✓	✓	-
32	315.286172	68.214544	0.234	0.83	0.33	0.67	0.18	✓	✓	✓
39	315.406921	68.191929	0.646	0.94	0.08	0.21	0.11	✓	-	✓
X-ray sources associated with the newly identified comoving sources										
c5	315.271092	68.072880	0.858	0.69	0.03	-0.08	0.03	✓	-	✓
c8	315.421356	68.182647	1.375	0.81	0.18	0.19	0.17	✓	-	✓
c9	315.439065	68.113329	0.081	0.88	0.04	0.06	0.05	✓	✓	✓
c14	315.501365	68.192470	0.123	0.98	0.09	0.44	0.10	✓	✓	✓
X-ray sources not associated with any of the known YSO candidates and comoving sources										
x1	315.169421	68.202133	-	-1.00	0.64	1.00	0.14	-	-	-
x2	315.376244	68.176781	0.243	0.63	0.17	0.43	0.12	✓	✓	✓
x3 [‡]	315.490013	68.036100	0.461	0.48	0.09	-0.54	0.10	✓	-	-
x4	315.722487	68.033205	0.651	0.44	0.10	-0.39	0.09	✓	✓	✓
x5	315.736835	68.128639	-	1.00	0.27	0.80	0.08	-	-	-

r is the separation of the position of sources detected in *XMM-Newton* and 2MASS.

[†] Star #13 is a double star (the second component is identified as 13b, see Table 3) of $\sim 2''$ separation as resolved by the *Gaia* DR2. However, in both *Spitzer* & *WISE*, they are detected as a single source. The *Spitzer* and the *WISE* values are assigned to the brightest of them.

[‡] There are two sources within a search radius of $5''$ from the X-ray detection.

Table 6. 2MASS, *Spitzer* and *WISE* magnitudes for the known YSO candidates and newly identified comoving sources with photometric quality ‘A’ in all bands.

#	RA	Dec	J±eJ	H±eH	K±eK	I1±eI1	I2±eI2	I3±eI3	I4±eI4	W1±eW1	W2±eW2	W3±eW3	Class
Previously known YSO candidates													
1	314.845315	68.245467	10.588±0.026	9.342±0.032	8.532±0.021	7.267±0.056	6.722±0.056	6.246±0.054	5.270±0.052	7.601±0.031	6.877±0.020	4.690±0.014	II
2	315.084447	68.140772	12.472±0.024	11.165±0.027	10.518±0.021	9.579±0.053	9.028±0.052	8.538±0.052	7.835±0.051	9.886±0.023	9.137±0.020	6.819±0.020	II
3	315.231481	68.190885	12.831±0.024	12.166±0.029	11.749±0.020	11.243±0.052	10.906±0.052	10.544±0.053	9.711±0.052	11.418±0.023	10.879±0.021	-	II
4 [†]	315.359984	68.177338	11.107±0.042	10.084±0.046	9.571±0.039	9.192±0.059	8.250±0.053	7.874±0.053	6.607±0.075	8.360±0.020	7.647±0.018	4.880±0.015	II
5 [†]	315.362884	68.177214	12.323±0.031	11.150±0.036	10.417±0.025	-	-	-	-	-	-	-	II
6 [‡]	315.399160	68.223752	12.471±0.029	11.033±0.038	10.257±0.023	9.139±0.054	8.579±0.056	8.536±0.052	7.538±0.053	9.355±0.023	8.649±0.020	-	II
7	315.400352	68.139576	-	-	-	10.166±0.054	9.404±0.053	8.988±0.060	7.663±0.087	9.844±0.023	9.114±0.020	-	Flat
8	315.403923	68.163263	6.111±0.030	5.465±0.031	4.651±0.017	-	-	-	-	-	-	-	-
9	315.427117	68.215960	11.911±0.031	10.892±0.033	10.421±0.023	9.752±0.056	9.466±0.059	9.090±0.053	8.388±0.054	9.905±0.023	9.400±0.020	-	II
10	315.444875	68.145894	11.792±0.024	10.798±0.033	10.159±0.022	9.561±0.052	9.246±0.051	9.144±0.052	8.760±0.054	-	-	-	II
11	315.558650	68.233141	13.982±0.032	12.405±0.033	11.686±0.024	10.870±0.052	10.513±0.058	10.179±0.055	9.496±0.053	11.065±0.023	10.513±0.020	-	II
12 [‡]	315.584979	68.423341	11.513±0.027	10.529±0.033	9.880±0.024	-	-	-	-	9.346±0.023	8.765±0.020	6.386±0.014	II
13*	315.617758	68.058287	-	-	-	9.350±0.055	9.001±0.053	8.526±0.066	7.495±0.054	9.103±0.022	8.630±0.020	6.637±0.016	II
13b*	315.618244	68.057669	-	-	-	-	-	-	-	-	-	-	-
14	315.637634	68.124746	11.559±0.027	10.713±0.029	10.411±0.021	9.614±0.054	9.282±0.053	8.937±0.053	8.347±0.052	9.905±0.023	9.452±0.020	8.021±0.028	II
15	315.747855	68.108939	13.871±0.035	13.083±0.033	12.357±0.028	10.772±0.055	9.968±0.053	9.069±0.052	7.279±0.054	11.302±0.023	10.105±0.020	5.962±0.015	I
16 [‡]	315.748555	68.136623	12.414±0.029	11.440±0.031	11.066±0.023	10.748±0.054	10.626±0.054	10.559±0.052	10.449±0.057	10.866±0.023	10.643±0.020	10.175±0.086	III
17	315.851719	67.985134	9.538±0.027	8.767±0.032	8.196±0.02	7.393±0.053	6.988±0.076	6.534±0.055	5.615±0.054	7.632±0.030	6.900±0.020	4.662±0.014	II
18 [‡]	315.923249	68.396018	13.762±0.029	13.020±0.037	12.603 ±0.030	-	-	-	-	12.189±0.023	11.762±0.020	10.090±0.035	II
19	315.997585	67.824847	12.789±0.029	11.981±0.031	11.478±0.019	10.618±0.055	10.225±0.052	9.909±0.052	9.284±0.053	10.838±0.023	10.231±0.020	8.685±0.021	II
Newly identified comoving sources													
c1	314.358914	68.184721	12.338±0.024	11.695±0.029	11.535±0.023	-	-	-	-	11.437±0.023	11.464±0.020	11.434±0.096	III
c2	314.877400	67.678993	12.772±0.025	12.145±0.030	11.769±0.026	-	-	-	-	11.531±0.023	11.201±0.020	11.006±0.069	III
c3	314.963955	68.336928	12.954±0.026	12.173±0.030	11.808±0.025	-	-	-	-	11.674±0.023	11.397±0.020	11.316±0.082	III
c4	315.201051	68.415148	11.715±0.026	10.773±0.030	10.495±0.019	-	-	-	-	10.386±0.023	10.349±0.020	10.172±0.041	III
c5	315.271845	68.072754	10.630±0.024	9.928±0.032	9.683±0.022	-	-	-	-	9.567±0.023	9.472±0.020	-	III
c6	315.350786	68.150243	13.516±0.024	12.851±0.029	12.411 ±0.022	-	-	-	-	-	-	-	-
c7	315.420625	68.301379	12.662±0.027	12.051±0.033	11.796±0.021	11.498±0.051	11.455±0.039	11.851±0.086	11.576±0.037	11.643±0.023	11.410±0.020	-	III
c8	315.422157	68.182326	12.300±0.029	11.373±0.033	10.854±0.022	-	-	-	-	9.575±0.020	9.220±0.019	-	II
c9	315.439309	68.113264	10.426±0.026	9.771±0.032	9.613±0.022	9.601±0.050	9.606±0.051	9.553±0.048	8.616±0.040	9.374±0.024	9.362±0.020	-	III
c10	315.450292	68.115938	13.893±0.027	13.136±0.033	12.739±0.025	12.217±0.094	11.903±0.042	10.789±0.064	9.414±0.050	11.447±0.025	11.002±0.022	-	II
c11	315.452017	68.135740	14.588±0.035	13.876±0.048	13.491 ±0.042	-	-	-	-	-	-	-	-
c12	315.458232	68.158415	12.589±0.024	11.948±0.032	11.573±0.023	-	-	-	-	-	-	-	-
c13	315.470563	68.362746	13.771±0.029	12.561±0.035	12.104±0.026	11.866±0.056	11.861±0.056	11.751±0.081	12.039±0.053	11.941±0.022	11.700±0.020	11.168±0.075	III
c14	315.501565	68.192440	11.968±0.027	10.816±0.032	10.387 ±0.019	10.257±0.056	10.161±0.050	10.123±0.053	10.217±0.045	9.939±0.022	9.748±0.020	-	III
c15	315.612647	68.015216	13.258±0.030	12.073±0.032	11.585±0.024	-	-	-	-	11.396±0.023	11.107±0.020	-	III
c16	315.675742	68.172632	14.368±0.035	13.549±0.037	13.125±0.024	12.465±0.052	12.217±0.052	12.004±0.084	10.621±0.050	12.366±0.023	12.051±0.023	-	II
c17	315.853497	68.132781	12.364±0.029	11.410±0.030	11.024±0.021	10.885±0.051	10.803±0.051	10.689±0.050	10.683±0.044	10.881±0.022	10.699±0.020	-	III
c18	316.150453	68.498418	11.570±0.030	10.782±0.037	10.454±0.023	-	-	-	-	9.746±0.023	9.338±0.020	7.241±0.016	II
c19	316.151474	68.496975	-	-	-	-	-	-	-	-	-	-	-
c20	316.394054	68.209051	11.600±0.027	10.918±0.031	10.626 ±0.021	-	-	-	-	10.559±0.022	10.511±0.020	10.342±0.042	III

[†] Stars #4 and #5 are resolved as two sources in 2MASS, *Spitzer* and *Gaia* DR2, but *WISE* detected them as a single source. We assigned the *WISE* to the brightest of them in K_s .

* Stars #13 & #13b appear as double sources of $\sim 2''$ in *Gaia* DR2. 2MASS classified it as an extended source. Visual inspection also show them as two sources. But detected as single source by 2MASS and *WISE*.

[‡] Stars 6, 12, 16 and 18 are identified as outliers based on our distance estimation.

Table 7. 2MASS, *Spitzer* and *WISE* magnitudes for the rest of known YSO candidates with photometric quality ‘A’ in all bands.

#	RA	Dec	J±eJ	H±eH	K±eK	I1±eI1	I2±eI2	I3±eI3	I4±eI4	W1±eW1	W2±eW2	W3±eW3	Class
20	314.137917	68.246667	14.583±0.077	13.669±0.087	13.275±0.072	-	-	-	-	12.204±0.023	12.118±0.021	9.304±0.026	II
21	315.078827	68.185074	15.386±0.058	14.533±0.065	13.994±0.066	-	-	-	-	13.749±0.026	13.681±0.029	-	III
22	315.086250	68.221111	-	-	-	12.255±0.059	10.343±0.058	9.331±0.051	8.501±0.051	12.086±0.023	9.698±0.020	7.528±0.018	I
23	315.089576	68.129234	-	-	-	-	-	-	-	-	-	-	-
24	315.092083	68.216111	-	-	-	11.207±0.063	9.391±0.055	8.462±0.051	7.576±0.051	11.595±0.027	9.086±0.021	7.028±0.017	I
25	315.093333	68.217778	-	-	-	12.755±0.069	11.520±0.059	10.883±0.053	10.089±0.053	-	-	-	Flat
26	315.120417	68.217222	15.998±0.080	13.096±0.030	11.584±0.023	10.270±0.055	9.756±0.053	9.321±0.051	8.585±0.051	10.587±0.023	9.638±0.020	8.006±0.022	II
27	315.133750	68.213056	11.377±0.024	9.836±0.028	9.096±0.021	8.379±0.052	8.053±0.050	7.688±0.052	7.143±0.053	8.712±0.022	8.143±0.020	6.690±0.016	II
28	315.152500	68.062222	11.646±0.022	10.826±0.027	10.608±0.023	10.391±0.056	10.394±0.052	10.318±0.052	10.191±0.051	10.458±0.023	10.377±0.020	-	III
29	315.242083	68.160556	12.389±0.026	11.535±0.031	11.081±0.020	10.539±0.051	10.225±0.052	9.802±0.055	8.935±0.051	10.623±0.023	10.116±0.021	-	II
30	315.262500	68.218611	14.118±0.040	12.755±0.043	11.969±0.029	11.028±0.050	10.448±0.055	10.165±0.052	9.293±0.053	-	-	-	II
31	315.265417	68.219167	-	-	-	10.171±0.054	9.761±0.054	9.432±0.051	8.733±0.053	9.877±0.023	9.305±0.020	-	II
32	315.286250	68.214444	14.736±0.034	13.627±0.037	12.902±0.032	12.189±0.052	11.764±0.052	11.317±0.054	10.568±0.069	12.385±0.024	11.675±0.022	-	II
33	315.292500	68.192500	14.764±0.036	14.097±0.041	13.677±0.047	13.091±0.053	12.779±0.055	12.384±0.060	11.660±0.071	-	-	-	II
34	315.302083	68.171944	11.829±0.027	10.836±0.035	10.391±0.022	9.786±0.054	9.542±0.056	9.098±0.054	8.202±0.058	9.839±0.022	9.386±0.020	-	II
35	315.363750	68.193889	15.378±0.059	13.15±0.037	11.806±0.025	10.578±0.053	10.093±0.053	9.508±0.054	8.667±0.050	10.728±0.023	9.842±0.020	-	II
36	315.365622	68.136520	13.999±0.024	13.195±0.031	12.663±0.029	-	-	-	-	11.455±0.036	10.664±0.029	-	II
37	315.373750	68.229444	14.116±0.039	12.398±0.038	11.410±0.022	10.442±0.052	10.023±0.056	9.520±0.049	8.856±0.053	10.852±0.023	10.086±0.021	-	II
38	315.386667	68.188889	-	-	-	12.404±0.057	10.778±0.057	9.726±0.052	8.599±0.061	11.507±0.022	9.835±0.019	-	I
39	315.406537	68.191931	11.271±0.024	10.260±0.031	9.683±0.022	-	-	-	-	8.935±0.022	8.474±0.020	-	II
40	315.431667	68.160000	11.218±0.024	10.415±0.030	10.156±0.020	9.988±0.054	9.951±0.052	9.859±0.058	9.961±0.075	-	-	-	III
41	315.432083	67.840556	13.056±0.027	11.82±0.031	11.090±0.022	10.300±0.051	9.992±0.054	9.756±0.053	9.129±0.053	10.478±0.023	9.915±0.020	8.335±0.021	II
42	315.432917	68.234167	15.036±0.071	13.734±0.052	12.402±0.032	9.872±0.052	9.045±0.055	8.376±0.051	7.840±0.051	10.040±0.023	8.894±0.018	-	I
43	315.439167	68.072500	13.281±0.026	11.923±0.031	11.352±0.025	10.796±0.057	10.368±0.060	10.209±0.056	8.886±0.055	11.002±0.023	10.515±0.020	-	II
44	315.469583	68.164167	-	-	-	11.058±0.051	10.319±0.057	9.741±0.060	8.744±0.064	-	-	-	II
45	315.478158	68.116402	14.116±0.032	13.264±0.035	12.664±0.023	-	-	-	-	11.534±0.025	11.490±0.021	-	II
46	315.510417	68.199444	14.854±0.043	13.549±0.036	12.878±0.030	-	-	-	-	12.319±0.024	11.796±0.023	-	Flat
47	315.553036	68.397097	11.573±0.024	10.469±0.032	10.099±0.021	-	-	-	-	9.937±0.023	9.956±0.020	9.791±0.034	III
48	315.558750	68.125000	15.768±0.075	14.656±0.056	13.604±0.044	11.397±0.056	10.438±0.054	9.683±0.057	8.435±0.064	11.263±0.024	10.167±0.021	-	I
49	315.588333	67.905556	-	-	-	10.772±0.055	9.363±0.054	8.566±0.053	7.728±0.052	11.389±0.022	9.111±0.020	6.931±0.016	I
50	315.592848	68.203369	-	-	-	-	-	-	-	-	-	-	-
51	315.613750	67.905000	-	-	-	13.589±0.063	12.985±0.066	13.105±0.081	13.139±0.101	-	-	-	Flat
52	315.616667	68.146389	15.574±0.059	13.815±0.046	12.786±0.036	11.894±0.053	11.418±0.054	10.940±0.054	9.914±0.052	-	-	-	II
53	315.624583	67.902222	15.022±0.074	12.035±0.038	10.415±0.024	8.621±0.054	7.938±0.055	7.392±0.051	6.733±0.059	9.131±0.023	7.971±0.020	6.271±0.015	II
54	315.645524	68.200684	15.337±0.051	14.377±0.056	13.685±0.050	-	-	-	-	-	-	-	-
55	315.728750	68.105833	15.661±0.067	13.712±0.041	12.261±0.023	10.688±0.051	10.240±0.053	9.945±0.054	9.329±0.055	10.809±0.023	10.033±0.020	-	II
56	315.781667	68.142778	12.435±0.029	11.398±0.032	10.732±0.021	10.035±0.052	9.690±0.050	9.372±0.053	8.632±0.053	10.134±0.023	9.627±0.020	7.494±0.026	II
57	315.800417	68.216944	-	-	-	-	-	-	-	-	-	-	-
58	316.065000	67.712778	6.256±0.019	5.068±0.018	4.616±0.017	6.100±0.178	4.499±0.060	4.042±0.071	3.892±0.061	-	-	-	III

The classifications of the YSO candidates were taken from Kirk et al. (2009).

α for #21, #36, #39, #45 and #47 were calculated by us.

This paper has been typeset from a \TeX/L\AA\TeX file prepared by the author.